

Pacific Southern Ocean coccolithophore-~~estimated~~derived particulate inorganic carbon (PIC) versus : ~~A novel comparative analysis of in-situ and~~ satellite-derived PIC measurements

Mariem Saavedra-Pellitero¹, Karl-Heinz Baumann², Nuria Bachiller-Jareno¹, Harold Lovell¹, Nele Manon Vollmar^{2,3}, Elisa Malinverno⁴

¹School of the Environment, Geography and Geosciences, University of Portsmouth, Portsmouth, PO1 3QL, United Kingdom

²Department of Geosciences, University of Bremen, 28334, Bremen, Germany

³NORCE Norwegian Research Centre AS, NORCE Climate & Environment, 5007, Bergen, Norway and Bjerknes Centre for Climate Research, Bergen, Norway

⁴Department of Geological Sciences and Geotechnologies, Milano-Bicocca University, 20126, Milan, Italy

Correspondence to: Mariem Saavedra-Pellitero (mariem.saavedra-pellitero@port.ac.uk)

Abstract.

Polar plankton communities are ~~already~~ experiencing the impact of ocean acidification and global warming. Coccolithophores are the main type of calcifying phytoplankton in the Southern Ocean (SO) and they play a key role in the carbon cycle through the production of particulate organic, and inorganic carbon (PIC). However, in situ ~~coccolithophore studies~~measurements of coccolithophores in the SO are sparse in space and time due to the harsh weather conditions. An alternative tool for monitoring PIC is- the use of optical remote sensing, because coccolithophores account for most of the optical PIC backscattering in the sea, ~~indicating that optical remote sensing presents an alternative tool for monitoring PIC, which makeso optical remote sensing ais~~ potentially an excellent monitoring tool. ~~However, in situ measurements in the SO are sparse in space and time due to the harsh weather conditions.~~ Here, we combine micropalaeontology and remote_sensing to evaluate ~~critical~~ discrepancies between coccolithophore and satellite-derived PIC in the Pacific SO (in non-bloom conditions). Plankton samples were collected ~~alongfrom~~ two latitudinal transects: from New Zealand to Antarctica (December 2004-January 2005) and across the Drake Passage (February-March 2016). ~~We compare Coccolithophore species-specific PIC estimates derived fromwere compared, based on~~ (1) Scanning Electron Microscope coccolith morphometric analyses and (2) MODIS-Aqua L2 and L3 MODIS-L2-remote-sensing-PIC concentration values-acquired from NASA's Ocean Color Web service. In general, the cS~~Considering that the SO is the cloudiest region on Earth (which limits the amount of satellite data available), satellite-derived PIC and coccolith-estimated PIC and satellite-derived PIC in-situ and satellite-derived PIC datasets, specifically a L-3 mapped~~

~~data product derived from MODIS Aqua sensor, show comparable trends in the Subantarctic and Polar Front Zones~~very good agreement in of both transects, with PIC-satellite values being- generally higher than coccolith-derived PIC. However, satellite data availability was impacted by cloud cover in the SO, particularly in the Subantarctic and Polar Front zones. According to the coccolithophorid data, *Emiliana huxleyi* morphogroup B substantially contributes to the sea-surface PIC content south of the Subantarctic Front in both transects, whereas *E. huxleyi* types A, type A overcalcified, and other taxa (e.g. *Calcidiscus leptoporus*), only contribute to coccolithophore PIC in the northernmost stations. ~~HO of particular interest are high strong peaks in satellite-derived PIC values south of the Polar Front, which are not apparent do not show up in the coccolithophore data. We suggest that the high reflectance signal at from their southernmost Antarctic Zone region (which could have been initially attributed to coccolithophores) may instead relate to the presence of be due to the prevalence of small biogenic opal particles, such as small size- (e.g. diatoms, silicoflagellates and/or small siliceous plankton) (as well as their fragments) small opal particles or or other as suggested by other authors, to unknown highly reflective particles (such as *Phaeocystis* aggregations or suspended sediment). Our results observations highlight the challenges presented by the lack of reliable satellite data in some parts of the SO; as well as the importance-relevance of importance of importance of the importance of in situ measurements and the importance of- methodological accuracy when estimating PIC values variables satellite products for estimating global PIC levels, and the while emphasizing the critical need for validation through field samples. This work contributes to our understanding of coccolithophore PIC dynamics in the “data desert” of the vast Pacific SO, offering valuable insights into for high-latitude the phytoplankton and zooplankton communities at high latitudes. for both remote sensing applications and the broader field of marine science.~~

1 Introduction

Coccolithophores are a major component of calcifying phytoplankton communities in the Southern Ocean (SO) (e.g. Saavedra-Pellitero et al., 2014; Saavedra-Pellitero et al., 2019; Malinverno et al., 2015; Charalampopoulou et al., 2016; Rigual Hernández et al., 2020a) and play an important and complex role in the carbon cycle through the production of particulate inorganic carbon (PIC) and particulate organic carbon (POC) (e.g. Rost and Riebesell, 2004; Salter et al., 2014). These haptophyte algae produce an external covering (coccosphere) of interlocking calcite platelets (coccoliths). This process decreases the alkalinity of surface waters, thereby reducing the uptake of CO₂ from the atmosphere into the surface ocean, and thus acting in opposition to carbon sequestration by the biological carbon pump (Rost and Riebesell, 2004). Previous work has suggested that calcification during blooms of the coccolithophore *Emiliana huxleyi*, aka *Gephyrocapsa huxleyi* (Bendif et al., 2023), might alter the air-sea flux of CO₂ (e.g. Harlay et al., 2010; Shutler et al., 2013), although to date, the impact of this has mostly only been explored on a limited regional basis (e.g. Holligan et al., 1993; Robertson et al., 1994; Balch et al., 2016).

Since the early days of satellite-based colour measurements of the oceans, large coccolithophore blooms have been visible as highly reflective regions in satellite images (e.g. Holligan et al., 1983). Coccolithophores, and their detached coccoliths, are strongly optically active and notably affect the optical budget of the surface ocean, and can thus be seen from space using satellite remote sensing (Smyth et al., 2002; Tyrrell and Taylor, 1996). Coccolithophores are responsible for most of the optical PIC backscatter in the ocean; the other, larger PIC particles associated with foraminifera and pteropods provide negligible backscatter per unit mass and therefore have minimal optical impact (Balch et al., 1996). In general, detached coccoliths account for 10-20-% of the light backscattered from the sea under non-bloom conditions, whereas under bloom conditions it can be more than 90-% (Balch et al., 1991; Balch et al., 1999). The strong scattering properties of the coccolithophores and the associated PIC lead to enhanced reflection in the entire visible spectrum (400-700 nm). Gordon et al. (2001) and Balch et al. (2005) developed algorithms to estimate the PIC concentration in the surface layer of the water column from the radiance emanating from the water. The relationship between inherent optical properties and the resultant light fields is well understood (e.g. Mitchell et al., 2017). The difficulty lies in understanding the combined effects of different in-water constituents on the inherent optical properties, and ultimately, the underwater light fields. While there have been many advances in this area (e.g. Babin et al., 2003a; Babin et al., 2003b; Devred et al., 2006), there will always be some uncertainty in calculating these relationships. For example, it has been shown that satellite ocean-colour-based PIC estimates did not match in situ (ship-based) observations and that satellite-derived PIC can be overestimated in Antarctic waters (e.g. Holligan et al., 2010; Trull et al., 2018). One potential source of error is that aquamarine waters characterized by high reflectance of light can also be caused by suspended sediment and even opal particles, such as fragments of diatom frustules (e.g. Broerse et al., 2003).

Satellite data has played a key role in showing the importance of the increasing *E. huxleyi* blooms in the world's oceans (e.g. Balch et al., 1991; Iida et al., 2002; Siegel et al., 2007; Neukermans et al., 2018; for further citations see the comprehensive review in Balch and Mitchell, 2023). This is relevant for monitoring changes at a global scale and to detect seasonal patterns as well as interannual variations (e.g. Smyth et al., 2004; Winter et al., 2014; Rigual-Hernández et al., 2020a) or trends, with the ultimate goal of feeding information into models for climate projections in the context of global warming and ocean acidification (e.g. Neukermans et al., 2018; Krumhardt et al., 2019). Recent concerns about climate change and ocean acidification pointed to *E. huxleyi* as a target cosmopolitan species to understand the biological response. Expansion or reduction of the biogeographic range, changes in coccolith calcification and preservation are possible responses that were observed in water and sediment samples. The high-latitude distribution of *E. huxleyi* has undergone a recent poleward expansion in both the northern (Rivero-Calle et al., 2015) and southern hemisphere (Cubillos et al., 2007; Winter et al., 2014). However, data from the SO is rather limited and there are currently not enough in situ measurements to unravel the complex dynamic relationships between *E. huxleyi* distribution and the frontal dynamics of the Antarctic Circumpolar Current (ACC). Significant zonal differences are shown in the relationship between coccolithophore data and ACC frontal positions across the

different sectors of the SO (e.g. Saavedra-Pellitero et al., 2014), but no strong evidence of recent expansion on a circumpolar scale has been identified (Malinverno et al., 2015).

The band of high reflectance and elevated PIC waters observed in the SO between 30°–60° S during Austral summer, known as “the Great Calcite Belt”, has been linked to a region of increased seasonal abundance/concentration of coccolithophores (Balch et al., 2011; Balch et al., 2016). Comparisons of in situ and remote sensing measurements of PIC have been undertaken in the Atlantic and Indian sectors of the SO for coccolithophore bloom conditions (e.g. Balch et al., 2014; Balch et al., 2016; Poulton et al., 2011). Nonetheless, this type of comparison is very limited in specific areas of the globe (such as the vast Pacific sector of the SO) but also in non-bloom coccolithophore conditions. This is partially due to the fact that available coccolithophore concentrations-measurements are sparse in space and time in the SO. Most-Many of the subpolar studies focus on coccospheres, whilst there are scarce data on free coccoliths (Mohan et al., 2008).

Changes in the calcification of *E. huxleyi* coccoliths have been shown in sub-Antarctic waters, (Cubillos et al., 2007), with different morphotypes representing the genotypic response to different water chemistry (Cubillos et al., 2007). Other studies (e.g., Beaufort et al., 2011; Horigome et al., 2014; Young et al., 2014) point to an environmental control on different calcification levels of *E. huxleyi*. Several estimates of coccolith-PIC exist; e.g.: estimation of coccolith-mass from coccolith volume calculated from coccolith-size (Young and Ziveri, 2000; Beuvier et al., 2019) or estimation of coccolith-calcite mass through calibration of its birefringence signal at the light microscope (Beaufort, 2005; Bollmann, 2014; Fuertes et al., 2014). Direct-comparisons between coccolith-estimated PIC and sea surface water scattering in the SO have targeted areas of coccolithophore blooms (Holligan et al., 2010; Poulton et al., 2011; Balch et al., 2014; Oliver et al., - 2023in press), but so far this has only occasionally been done/not been undertaken for non-bloom areas (e.g. Oliver et al., 2023).

Here, we focus on/calculate the contribution of *E. huxleyi* and other coccolithophore taxa to sea surface PIC along two latitudinal transects across the ACC fronts: a New Zealand transect (December 2004-January 2005) and a Drake Passage transect (February-March 2016). Where coccosphere concentrations in the New Zealand transect were below 1.43×10^5 cells/L and in the Drake Passage transect were below 1.5×10^5 cells/L, respectively corresponding to non-bloom to outer bloom conditions (Poulton et al., 2011). Our aims are: (1) to estimate the contribution of different coccolithophore taxa and morphotypes to PIC and (2) to compare coccolith-based PIC estimates with satellite-derived PIC values in the Pacific SO. (1) to compare coccolith-based PIC estimates with satellite-derived PIC values in the Pacific SO and (2) to assess the contribution of the different coccolithophore taxa to the calculated PIC. 1) to define the contribution of the different coccolithophore species to PIC in surface waters, 2) to assess the degree of calcification of the different *E. huxleyi* morphotypes along the transect and 3) to assess the source of high reflectance in the Antarctic Zone, south of the Southern ACC Front, along our investigated transect.

2 Study area: Oceanographic setting and, phytoplanktonic communities, and study area

The SO is a high-nutrient, low-chlorophyll area in the Southern Hemisphere (e.g. De Baar et al., 1995) that connects all the main oceans through the strong and eastward flowing ACC. In the SO, there are a number of oceanographic fronts characterized by increased horizontal transport and rapid changes in water properties (Orsi et al., 1995; Klinck and Nowlin, 2001). The ACC is bounded by the Subtropical Front (STF) in the north, which separates it from the warmer and saltier waters of the subtropics, and its southern edge is marked by the Southern Boundary, which separates it from subpolar cold, silicate-rich waters (Orsi et al., 1995). Although the ACC flow is mostly driven by the westerly winds, the position of the fronts varies spatially and seasonally and it is also controlled by steep topographic features, such as oceanic plateaus or ridges (Gordon et al., 1978). South of the STF, the Subantarctic Front (SAF) separates the Subantarctic Zone (SAZ) and the Polar Frontal Zone (PFZ) (Fig. 1). The location of the SAF is indicated by a strong thermal gradient and by the rapid descent of a salinity minimum associated with the Antarctic Intermediate Water, from the surface in the PFZ ($S < 34.20$ ‰) to depths greater than 300 m in the SAZ ($S < 34.20$ ‰) (Orsi et al., 1995; Whitworth, 1980). South of the SAF, the prominent Polar Front (PF) separates the PFZ and the Antarctic Zone (AZ). The PF represents the northernmost extent of the 2°C isotherm at 200 m depth and corresponds to a 2°C gradient in sea surface temperature (Orsi et al., 1995). The Southern ACC Front is characterized by temperatures below 0°C at the minimum temperature in the sub-surface (<150 m) and above 1.8°C at the maximum temperature at depths >500 m (Orsi et al., 1995). A more detailed description of the property indicators at each SO front can be found in Orsi et al. (1995).

Coccolithophores dominate the SO phytoplankton communities, especially in the SAZ, where they reach relatively high numbers and diversity (e.g. Gravalosa et al., 2008; Saavedra-Pellitero et al., 2014; Malinverno et al., 2015; Charalampopoulou et al., 2016; Saavedra-Pellitero et al., 2019; Rigual Hernández et al., 2020a). On the other hand, diatoms and other siliceous microfossils dominate south of the PF (e.g. Saavedra-Pellitero et al., 2014; Malinverno et al., 2016; Cárdenas et al., 2018). The coccolithophore abundance and diversity in the Drake Passage drastically drop from north to south, with the oceanographic fronts appearing to act as ecological boundaries (Saavedra-Pellitero et al., 2019), whereas the total coccolithophore abundance is highest in the PFZ south of New Zealand (Malinverno et al., 2015). Similar marked shifts at the SAF and PF in coccolithophore number, community composition, and diversity occurring were also previously noted in other sectors of the SO (e.g. Mohan et al., 2008; Gravalosa et al., 2008; Holligan et al., 2010; Saavedra-Pellitero et al., 2014; Balch et al., 2016; Charalampopoulou et al., 2016) and are in accordance with previous observations in both transects (Malinverno et al., 2015; Saavedra-Pellitero et al., 2019). In particular, the PF (Drake Passage) and the Southern ACC Front (New Zealand transect) constitute natural sharp barriers marked by a clear drop in the number of *E. huxleyi*, which often is the only species found in the PFZ and almost always ~~or only~~ occurs here as B morphogroup (types B/C and O). Furthermore, a general southwards decreasing trend in *E. huxleyi* mass, linked to a latitudinal trend from more calcified *E. huxleyi* (A morphogroup) to weakly calcified morphotypes (B morphogroup), was already recorded across the Drake Passage (Saavedra-Pellitero et al., 2019).

3 Materials and methods

3.1 Sampling considerations and morphometrics

3.1.1 The New Zealand transect

Forty-twoFifty-eight surface water samples were collected from the ship's pump of the *R/V Italica* (at ca. 3 m water depth) from 46.81°S to 69.3798°S during the XX Italian Expedition from New Zealand to Antarctica from (31st December 2004 to- 6th January 2005,) and withand 42forty-two were considered in this study (Fig. 1, Table 1). Details on sample locations, sampling volume, coccolithophore and coccolith counts can be found in Malinverno et al. (2015).

From these samples, we selected a total of 13 water samples for Scanning Electron Microscope (SEM, Vega Tescan at the University of Milano-Bicocca) morphometric analyses of *E. huxleyi* coveringas being representative of the different *E. huxleyi* populations from the various biogeographic zones across the ACC (Fig. 1). For each sample, 30-50 images of *E. huxleyi* free coccoliths and coccospheres were collected as encountered during filter scanning (377 images in total, Table 1S in Supplementary Material). Distal shield length and width, tube thickness, and number and thickness of distal shield elements were manually measured using the ImageJ software (Schneider et al., 2012) in micrometers (μm) using the scalebar of the SEM images (Fig. 2).

3.1.2 The Drake Passage transect

Nineteen water samples were collected on a transect at the western end of the Drake Passage (55.44°S to 61.75°S) during the *Polarstern* Expedition PS97 from 24th February 2016 to 5th March 2016 (Fig. 1, Table 1). These selected plankton samples were obtained using a rosette sampler with 24×12 L Niskin bottles (Ocean Test Equipment Inc.) attached to a CTD Seabird SBE911plus device (Lamy, 2016). The bottles were fired by a SBE32 carousel and just the shallowest samples, from 5, 10 and 20 m water depth, were considered in this work. Details on sample locations, sampling volume, coccolithophore assemblages and coccospheres/L can be found in Saavedra-Pellitero et al. (2019).

A total of 203 images of *E. huxleyi* coccospheres were taken from the samples in the Drake Passage while scanning the filters within anotherthe SEM (Zeiss DSM 940A at the Geosciences Faculty, University of Bremen; Table 2S in Supplementary Material). Coccoliths were measured using the Coccobiom2 macro (Young, 2015) in the software programme Fiji, an image processing package based on ImageJ (Schindelin et al., 2012). Measurements were made in micrometers (μm), based on the scale bar of the SEM images. Note that they were scaled to 100% with a Coccobiom2 SEM calibration of 1.09 and the specific magnification.

3.2 Coccolithophore PIC estimates

Species-specific coccolith-PIC (in pmMol) was estimated following the volume calculation of Young and Ziveri (2000)

Formatted: Font: Italic

Formatted: Font: Italic

$$PIC = 2.7 \times Ks \times L^3 \div 100 \text{ [equation 1]}$$

where:

2.7 = density of calcite;

Ks = species-specific shape factors, as provided by Young and Ziveri (2000) and modified for *E. huxleyi* according to the degree of calcification obtained for each morphotype as compiled by Vollmar et al. (2022) (further details insee Table 24);

L = coccolith mean length from measurements in the case of *E. huxleyi*. For minor species, we considered the averaged coccolith length provided by Young and Ziveri (2000);

100 = molecular weight of calcite.

Measurements of the distal shield diameters of *Calcidiscus leptoporus*, the second most abundant species, that is significantly larger and much more massive than *E. huxleyi*, were made on different samples offshore of New Zealand, corresponding to the highest abundances of this taxa (Table 24 and Table 3S in Supplementary Material). The importance of own size measurements for the determination of species-dependent coccolith PIC has been clearly emphasized (Baumann, 2004). The coccolith-PIC contribution for each sample was calculated by applying the obtained species-specific calcite quota to the abundances of species and morphotype (i.e., coccospheres/L) from Malinverno et al. (2015) and Saavedra-Pellitero et al. (2019) (Tables 1 and 2). In the New Zealand transect, the single / double coccolith layers were considered in the estimates (Table 1S in Supplementary Material), while in the Drake Passage transect, where this information was not available, an average was considered based on our own observations (Table 24 and Table 4S in Supplementary Material). Additionally, detached coccoliths/L were considered for the PIC estimates in the New Zealand transect (Malinverno et al., 2015). To estimate the number of coccoliths per coccosphere we counted the visible placoliths (half coccosphere) and multiplied by two (e.g. Table 4S).

We also calculated the relative tube width² in *E. huxleyi* as a size-independent index to estimate the degree of calcification in this taxa following a modification of the index proposed by Young et al. (2014) (Fig. 2):

$$\text{Relative tube width}' = (2 \times \text{tube width}) \div \text{coccolith length}$$

$$\text{Relative tube width} = (2 \times \text{tube width}) \div \text{coccolith width} \text{ [equation 2]}$$

Note that because the relative tube width is a ratio, it is dimensionless and it should be size-independent (Young et al., 2014).

3.3 Coccolith-estimated PIC errors

There are series of errors and uncertainties linked to the approach chosen to estimate the coccolith PIC. To assess the reproducibility of the measurements, two different coccoliths were measured 50 times each. The standard deviation (SD) for the coccolith length was 0.014 and 0.017 μm and the standard error 0.002 μm in both cases. Coccolith volume estimates are likely to contain errors around 40-50% according to Young and Ziveri (2000), so we assumed the largest potential error and added a 50% error bars to our plots, although we note that even if measuring the actual size range in the sample can reduce this error to about 5-10% in length and 15-30% in volume.

3.4 Satellite-derived PIC and chlorophyll a data and errors processing

To compare the coccolith-estimated PIC with satellite-derived values, PIC concentration in mol m^{-3} was obtained from the MODIS-Aqua Level (L) 2 and L3 products (NASA Goddard Space Flight Center, Ocean Ecology Laboratory, Ocean Biology Processing Group, 2022a). To encompass the broad range of PIC concentrations observed in the global ocean, a combination of two independent approaches is used to calculate the backscattering coefficient for PIC (b_{PIC}) (the description of the algorithm can be found in NASA Ocean Biology Processing Group, 2023; for further details see also Balch and Mitchel, 2023-). The Ocean Biology Processing Group (OBPG) validates MODIS-Aqua PIC retrievals against in situ measurements, which results in a mean bias of ± 0.31623 and a mean absolute error (MAE) of ± 3.91664 (both values calculated based on \log_{10} transformation to the PIC values) (<https://oceancolor.gsfc.nasa.gov/data/reprocessing/r2022/aqua/>). These metrics indicate the degree of accuracy and potential bias in the satellite-derived estimates compared to direct observations.

MODIS-Aqua L2 scenes encompassing both the sampling period and the geographical extent of each transect, were downloaded from NASA's Ocean Colour Level 1 and L2 browser (<https://oceancolor.gsfc.nasa.gov/cgi/browse.pl>). The downloaded MODIS L2 scenes corresponded to swaths covering including at least 50-% of the study area and included more than one daily scene. Table 3 summarizes the number of downloaded scenes as well as their time coverage. To obtain satellite-derived PIC concentrations for comparison with coccolith-estimated PIC at each sample location, the PIC concentrations estimated from coccolith counts at each station, the mean of a 5x5 window centered on the measurement location (Bailey and Werdell, 2006) was extracted from the downloaded scenes using the SNAP 9.0.0 pixel extraction tool (European Space Agency (ESA), 2022). This tool also provides basic statistics, such as the number of pixels (N) contributing to each mean value and the standard deviation (SD) of these pixel values, allowing to assess the homogeneity of the extraction point to be assessed. Pixels flagged with atmospheric correction failure (ATMFAIL) or very low water-leaving radiance (LOWLW) were excluded from the extraction. The output file from the SNAP tool was then uploaded to the JASMIN

~~Jupyter notebook service for further analysis.~~ To ensure statistical confidence in the ~~values~~-retrieved values, all PIC mean values resulting from the aggregation of 12 or fewer N within the 5x5 window were discarded (Bailey and Werdell, 2006). ~~Then, duplicate daily mean PIC^{pie} values (i.e. PIC^{pie} values for a measuring location extracted from more than one scene captured on the same day) and their corresponding SD^{std} were then combined with weighted~~s according to ~~based on~~ their uncertainties (Bevington, 1969) to give more prominence~~relevance~~ to measurements with a lower SD~~std~~, which are generally considered to be more reliable. However, daily mean values with SD equal to zero were used directly as the result, since the value with zero SD suggests homogeneity.

Due to high cloud cover and other conditions that interfere with the detection of water-leaving radiances (NASA Ocean Biology Processing Group, 2023), daily PIC grids yielded a high number of missed observations, or gaps, which prevented us from acquiring~~getting~~ daily satellite-derived PIC values of the sampling dates for most sample locations in both transects (Figs. ~~ures~~ 1S and 2S in Supplementary Material show the availability of MODIS-Aqua L2 PIC values across stations over the sampling period). This data scarcity made it impossible to use a time window of 24 hr to determine coincidence between coccolith-estimated PIC~~measures~~ and satellite-derived PIC~~estimates~~. Therefore, to increase data availability, we (1) extended the satellitesampling period to seven days before and after sampling dates (see Table 3 for specific dates) and extracted the PIC for all sample locations~~stations~~, regardless of their sampling date. We deliberately chose that time range -considering that *E. huxleyi* can double its numbers in two~~2~~ or three~~3~~ days without accounting for grazing by zooplankton (based on studies in the North Atlantic; Holligan et al., 1993), ensuring no drastic changes from non-coccolithophore bloom to bloom conditions. We then generated a mean PIC value for each location by aggregating the available daily means over the full period to explore the latitudinal variation of this variable; and (2) also obtained monthly (Figs. 3S and 4S in Supplementary Material) and 8-daily (going forward, referred to as weekly) satellite-derived PIC concentrations (mol m⁻³) from the MODIS-Aqua L-3 product (NASA Goddard Space Flight Center, Ocean Ecology Laboratory, Ocean Biology Processing Group, 2022b). This allowed us to have additional satellite-derived PIC values to compare to the coccolith-estimated PIC in the study area. Images encompassing both the sampling period and the geographical extent of each transect, were acquired from NASA's Ocean Color Level 3 and 4 Browser (<https://oceancolor.gsfc.nasa.gov/l3/>) as 4 km cell size gridded files in NetCDF file format. Table 3 summarizes the number of downloaded scenes as well as their time coverage. The L3 extracted values corresponded to the PIC concentration of the grid cell enclosing the sample location. As per L2 data extraction, PIC concentrations for all sample locations were acquired from all available monthly and weekly scenes. ~~—~~

MODIS-Aqua L2 chlorophyll a ~~(CHL)~~ concentration in mg m⁻³ were also extracted and processed as an ~~because chlorophyll a concentration is an important~~ indicator of the presence of diatoms and other phytoplanktonic groups~~taxaspecies~~, as described above for PIC. ~~The~~ The algorithm used to calculate chlorophyll a~~CHL~~ is documented by Werdell et al. (2023). Chlorophyll~~CHL~~ concentration is an important indicator of the presence of diatoms and other phytoplankton speci

Formatted: Font: Italic

Formatted: Font: Italic

Formatted: Superscript

Monthly and 8-daily (going forward, referred to as weekly) satellite-derived PIC concentrations (mol m^{-3}) were obtained from MODIS-Aqua L-3 product (NASA Goddard Space Flight Center, Ocean Ecology Laboratory, Ocean Biology Processing Group, 2022b). Images encompassing both the sampling period and the geographical extent of each transect, were acquired from NASA's Ocean Color Level 3 and 4 Browser (<https://oceancolor.gsfc.nasa.gov/l3/>) as 4 km cell-size gridded files in NetCDF file format. Tables 3 summarizes the number of downloaded scenes as well as their time coverage.

The L3 extracted values corresponded to the PIC concentration of the grid cell enclosing the measuring station. As per L2 data extraction, PIC concentration for all stations was acquired from all available monthly and weekly scenes. Latitudinal variations of monthly and weekly MODIS-Aqua LC derived PIC are shown in figures 3(b) and 4(b). The L3 PIC extraction was done in JASMIN Jupyter notebook service.

Daily L2 and Ddaily, 8-daily (from now ongoing forward, referred to as weekly) and monthly L-3 MODIS-Aqua-derived PIC concentration values (mol m^{-3}) (NASA Goddard Space Flight Center, Ocean Ecology Laboratory, Ocean Biology Processing Group, 2014;)(NASA Ocean Biology Processing Group, 2022, 2023a) with a spatial resolution of 4 km, covering both the sampling period and the geographical extent of each transect, were acquired from NASA's Ocean Color Web service as 1 km and 4 km cell-size gridded files in NetCDF file format individual netCDF files for each timestamp. The date ranges and spatial resolution of each PIC data product period are summarised in Table 32. NASA Ocean Biology Processing Group validates PIC retrievals performed with available matchups returns mean bias of 0.30577 and mean absolute error of 4.00304 (both values — calculated — after — applying — the — \log_{10} — transformation — to — the — PIC — values) (<https://oceancolor.gsfc.nasa.gov/data/reprocessing/r2022/aqua/>). MODIS L2 downloaded on 10/07/2024. The downloaded scenes corresponded to swaths including at least 50% of the AOI.

Downloaded files
17-02-2016 / 12-03-2016
total num files 50
24-12-2004 / 13-01-2005
total num files 34

Pixel extraction files done using SNAP 9.0.0 (work version) on 17/07/2024. Extractions include 5x5-MEAN excluding pixels flagged with 12-flags.ATMFAIL OR 12-flags.LOWLW for the images listed below.

NOTE: These downloaded images corresponded to swaths including at least 50% of the AOI — they were downloaded on 10/07/2024

Daily, 8-daily (going forward, referred to as weekly) and monthly values of PIC were extracted for all sampling locations in both transects (Figures 1S and 2S in Supplementary Material). Processing of the PIC data was done with a Python script that

used NetCDF4 and other libraries commonly used for data analysis such as Pandas. The PIC data processing was done in JASMIN Notebook Service (<https://jasmin.ac.uk/>). To compare the satellite-derived PIC to the coccolithophore estimates, the mean of a 5x5 window centered on the measurement location (Bailey and Werdell, 2006) was extracted from MODIS L2 daily grids using SNAP 9.0.0 pixel extraction tool which generates a text file that was subsequently processed using a Python script. Due to high cloud cover One limitation of optical satellite-borne sensors remote sensing products is that they cannot provide a reliable signal under cloudy conditions. Combined with and other atmospheric conditions that interfere with the detection of water-leaving radiances (NASA Ocean Biology Processing Group, 2023a), daily PIC grids yielded a high number of missed observations, or gaps, which prevent us from getting daily satellite-derived PIC values of the sampling dates for most sample locations in both transects (Figures 3SX and 4SX in Supplementary Material show the availability of MODIS L2 PIC values across the sampled stations over the period of interest). Consequently, after discarding 5x5 mean PIC values calculated with fewer than 13 values, the remaining daily means at each station were averaged over the sampling period of the transects. Figures 3X and 4X show the latitudinal trend of both satellite and coccolithophore PIC estimates. Additionally, Based on this fact, weekly and monthly and weekly MODIS L3 satellite-derived PIC values were therefore used in the analysis. Monthly and 8 daily (going forward, referred to as weekly) and monthly values of PIC were extracted for all sampling locations in both transects (Figures 31S and 42S in Supplementary Material). The PIC values extracted corresponded to the PIC concentration of the grid cell enclosing the measuring station. The processing of the PIC data was done with a Python script. PIC. Latitudinal variation of monthly and weekly PIC are shown showing in figures 3, 4 and 1S and 2SX, X.

The PIC data processing was done in JASMIN Notebook Service (<https://jasmin.ac.uk/>).

3.5.4 Statistical analysis

In order to explore potential relationships between coccolith morphometrics and morphotype composition of *E. huxleyi* in the study area, a principal component analysis (PCA) was performed on the *E. huxleyi* morphometric dataset (including samples from both transects) using PASTTM software version 4.13 (Hammer et al., 2001). The morphometric data considered here (including samples from both transects) were: coccolith length, coccolith width (minor), distal shield element (or T-element) width, number of T elements and tube width measurements. The main aim of the PCA is to find hypothetical components that account for the maximum variance in the multivariate dataset (Davis, 1986; Legendre and Legendre, 1998; Harper, 1999). These components are linear combinations of the original variables (Hammer et al., 2001). The first Principal Component explains the highest variance, followed by the subsequent components which explain the next largest variances. All the measurements were log-transformed prior to the PCA to avoid skewness.

Formatted: Font: Italic

4 Results

4.1 Coccolith-estimated PIC versus satellite-derived PIC

Emiliana huxleyi is clearly the dominant species in the coccolithophore assemblage of the Pacific SO (Malinverno et al., 2015; Saavedra-Pellitero et al., 2019) with abundances of 1.4×10^5 coccospheres/L (at station TR033) right south of the SAF in the New Zealand transect and 1.5×10^5 coccospheres/L (at station PS97/034-2) in the Drake Passage Chilean SAZ (PS97/034-2) and it is also the main contributor to sea-surface PIC (Figs. 3 and 4). *Calcidiscus leptoporus* (mostly the intermediate-sized form) is the second most abundant species and makes significant contributions to the coccolithophore PIC at certain locations (up to 1.4×10^4 cells/L in the New Zealand transect and 1.4×10^3 cells/L in the Drake Passage, Figs. 3 and 4) (Malinverno et al., 2015; Saavedra-Pellitero et al., 2019). *Calcidiscus leptoporus* generally represents on average 20.2-43.4% of the total coccolithophore PIC in the New Zealand transect and 5.33-8% in the Drake Passage, but can occasionally reach maximum PIC contributions of 68.357-5% (at station the-TR0087-station, in the SAZ) and of 31.123-3% (at the station PS97/01738-1, in the SAZ/PFZ) (Fig. 5).

A minor contribution from less abundant or rare species is found occurs just in the northern SAZ of both transects, where diversity is higher (for species list see Malinverno et al., 2015; Saavedra-Pellitero et al., 2019), with a poleward decreasing trend and almost no contribution south of the SAF (Fig. 5). *Emiliana huxleyi* is solely responsible for almost all of the coccolith-estimated PIC in the PFZ, but its contribution decreases at the PF (in the Drake Passage) and at Southern ACC Front (in the New Zealand transect, ca. 63.7°S) and further south of it.

Daily, L2, weekly and monthly satellite (MODIS-Aqua L2) MODIS-Aqua-derived MODIS-derived PIC at the sampling locations are generally consistently overestimate higher than coccolith-estimated PIC estimates in both transects; this difference is larger in the Drake Passage (Fig. 4) than in the New Zealand transect (Fig. 3). estimates values by a factor of 2 to 5 with respect to in-situ values calculated from coccolith mass in the New Zealand transect (Fig. 3) and by occasionally an order of magnitude in the Drake Passage (Fig. 4). There are Apart from the discrepancies in absolute values (on top of the and considering that there are already inherent variations in the weekly compared to the monthly PIC estimates and the limited availability of L2 data available).; These which are became particularly obvious there is a relatively good agreement in the latitudinal satellite and coccolith-PIC trends in the SAZ and PFZ.

However at the PF (ca. 60°S in the Drake Passage) or to the south of it (ca. 62.5°S in the New Zealand transect), where the satellite-derived and the coccolith-estimated coccolith-estimated PIC estimates became decoupled, characterized by with high reflectance but no coccolithophores in the AZ.

4.2 Morphometries and mass estimates of *Emiliania huxleyi*

Emiliania huxleyi consist of different morphotypes that show a different and partly overlapping distribution along both latitudinal transects (Malinverno et al., 2015; Saavedra-Pellitero et al., 2019). Type A is mostly restricted to the northern SAZ, but it is occasionally present in the PFZ in the Drake Passage (Figs. 3, 4) and it is the only type within morphogroup A in this study. Morphotypes belonging to the *E. huxleyi* morphogroup B (which includes morphotypes B, B/C, C and O) are present in the SAZ and the PFZ, but they disappear south of the PF.

Morphometric measurements on coccoliths of *E. huxleyi* from the selected samples show that the length of types A, B/C-C and O overlap in both transects (Fig. 6). In the Drake Passage, coccolith lengths range from 2.86 to $3.96 \pm 0.43 \mu\text{m}$ (unless specified, \pm refers to the SD from now on) μm , with a mean average of $3.49 \pm 0.33 \mu\text{m}$ for A type (including normal and overcalcified specimens), 2.87 to $4.11 \pm 0.45 \mu\text{m}$ for B type, 2.20 to $3.98 \pm 0.37 \mu\text{m}$ for B/C-C types, 2.42 to $4.16 \pm 0.41 \mu\text{m}$ for O type, and an average of $2.98 \pm 0.40 \mu\text{m}$ for morphogroup B. In the New Zealand transect, maximum lengths range from 2.25 to $3.59 \mu\text{m}$, with an average of $2.95 \pm 0.28 \mu\text{m}$ for *E. huxleyi* A-type A, 1.95 to $3.62 \pm 0.33 \mu\text{m}$ for B/C-C types, 2.07 to $4.14 \pm 0.36 \mu\text{m}$ for O-type O, and an average of $2.87 \pm 0.35 \mu\text{m}$ for morphogroup B.

Figure 65 provides a latitudinal overview of morphometric data compared to the (averaged) degree of calcification (indicated by the dimensionless relative tube width index; Young et al., 2014). In the New Zealand transect there are no significant changes in coccolith lengths except for a wide scatter of values characterizing the size class distribution of each sample. This feature reflects the large variability in coccoliths size as observed on coccoliths from a single coccosphere (Fig. 2e). However, in the Drake Passage transect, *E. huxleyi* coccoliths are notably larger offshore of Chile (Fig. 6a).

Emiliania huxleyi masses calculated in the New Zealand transect range from 0.61 to 2.93 pg with an average of $1.47 \pm 0.46 \text{ pg}$ per coccolith belonging to the morphogroup A, and from 0.36 to 2.86 pg , with an average of $1.15 \pm 0.43 \text{ pg}$ per coccolith from morphogroup B (Fig. 3ee). In the Drake Passage the masses per coccolith for morphogroup A are almost double than in the New Zealand transect, varying between 1.394 pg and 6.263 pg , with an average of $3.00 \pm 1.19 \text{ pg}$. The coccolith masses in morphogroup B range from 0.576 to 3.75 pg with a mean of $1.44 \pm 0.62 \text{ pg}$ across the Drake Passage (Fig. 4ee).

Note that this data is shown in Figures 3 and 4, but

To estimate the coccolith PIC, was calculated equation 1 and the average lengths mentioned in Table 2 were used. in this work using equation 1 and the average lengths mentioned in Table 1. The coccolith-estimated PICs estimated for just the species *E. huxleyi* are generally lower in the New Zealand transect (average morphogroup A: $0.021 \pm 0.010 \text{ pmol}$ and B: $0.013 \pm 0.006 \text{ pmol}$, considering 50% potential error) than in the in the Drake Passage (average morphogroup A: $0.034 \pm 0.017 \text{ pmol}$ and B: $0.014 \pm 0.007 \text{ pmol}$ -error-).

We observed that some coccoliths are clearly overcalcified (see Fig. 65 for an example), with a thick inner tube (up to 0.76 μm in sample PS97/018-1) that extends into the central area. Specimens belonging to the morphogroup A show a higher degree of calcification than those belonging to morphogroup B, resulting not only in a thicker inner tube but also in thicker distal shield T-elements. The overcalcified coccospheres co-occur with normally-calcified ones but they are restricted to the northernmost samples (Fig. 6). The relative tube width² (as an index for calcification; Young et al., 2014), calculated using equation 2, varies from 0.1098 to 0.28 ± 0.042 in morphogroup A and from 0.076 to 0.2148 ± 0.03 in B for the New Zealand transect. Values are higher in the Drake Passage, ranging from 0.054 to 0.5041 ± 0.12 for *E. huxleyi* morphogroup A, and from 0.02 to 0.2249 ± 0.04 for morphogroup B.

The degree of variation in the degree of calcification (calculated using equation 2) is highly variable within each sample of the New Zealand transect (Fig. 3db), but although overcalcified specimens (relative tube width² > 0.232), typically represented by type A, only occur in the northernmost samples (Fig. 6b). The averaged relative tube width index² shows increased values not only in the SAZ offshore of New Zealand, but also around 54°S and in the PFZ (Figs. 3d, 6b), which points to a certain degree of variation in the calcification within morphotypes BC/C and O. A more marked N-S decrease in the relative tube width index² values is observed in the Drake Passage, with notably higher values offshore of Chile (Figs. 4d3b and 6a), where relatively large and heavily calcified type A coccospheres are present.

To better characterize *E. huxleyi* morphotypes in the study area we performed a PCA of the log-transformed morphometric data. The first component, related to the tube width, explains 79.9% of the variance, and the second, related to length as well as width (and to a lesser extent distal shield element width and number of T-elements), accounts for 11.5% (Fig. 7).

5. Discussion

5.1 PIC variability in the SAZ and PFZ

In the studied transects, even with the limited data available, the calculated coccolith-estimated PIC and the satellite-derived PIC show a comparable trends show quite good agreement in the SAZ and PFZ, but there is a strong discrepancy in the AZ (Fig. 5S in the Supplementary Material). Here we discuss potential factors influencing water-leaving radiance in each of those areas. The fact that satellite-derived PIC is generally higher data generally show higher values than coccolith-estimated PIC estimates in the SAZ and PFZ (Figs. 3, 4 and 5S in the Supplementary Material) could be due to an underestimation of the species specific coccolith-estimated PIC. The potential assumptions linked to the coccolith-estimated PIC estimates, including shape factors (Ks), average coccolith length (L), number of coccoliths per coccosphere, and/or number of coccolith layers per cell (Table 2), have associated uncertainties associated. Even if we tried to minimize these by measuring the actual coccolith size range and counting coccoliths per

coccosphere (instead of using assumed values), the overall error can still add up to $\pm 50\%$ (Young and Ziveri, 2000). Additionally, the fact that the difference between satellite-derived PIC and coccolith-estimated PIC estimates in the Drake Passage transect is larger than in the New Zealand transect can be also in part attributed to the fact that detached coccoliths (in addition to coccospheres) were only considered in the estimates for the New Zealand transect.

Given that *E. huxleyi* is the dominant species and the main contributor to the coccolith-estimated PIC in the SAZ and PFZ of both transects (Fig. 5), we focused on its abundance, morphotype distribution and calcite weight to assess potential PIC discrepancies. Coccolith-estimated PIC calculated in this study for *E. huxleyi* are generally in agreement with the calcite content per coccolith obtained by Poulton et al. (2011) along the Patagonian Shelf and by Rigual Hernández et al. (2020a) in the Australian and New Zealand sectors of the SO (see Tables 1 in those papers). Our *E. huxleyi* PIC estimates seem generally higher than the estimates by Charalampopoulou et al. (2016) off southern Chile ($0.015 \text{ pmol per coccolith}$) and across the rest of Drake Passage ($< 0.009 \text{ pmol}$).

On the other hand, our values are slightly lower than those obtained through the birefringence method SYRACO, an automated system of coccolith recognition (SYstème de Reconnaissance Automatique de COccolithes) in the same latitudinal range (e.g. Beaufort et al., 2011), and notably lower than Saavedra-Pellitero et al. (2019), who used across the Drake Passage using circularly polarized light plus the C-Calcita software developed by Fuertes et al. (2014) across the Drake Passage (Fig. 7a). In order to explore this difference, we calculated PICs in the Drake Passage using the Saavedra-Pellitero et al. (2019) mass estimates for the same samples, considering an average mass of $4.64 \pm 2.53 \text{ pmol}$ for *E. huxleyi* ($n = 796$), but without distinguishing different morphotypes (Fig. 7c). The mass per coccolith of *E. huxleyi* using C-Calcita in the Drake Passage is 2.8 times higher than in this studywork (mean of $1.66 \pm 0.91 \text{ pg}$ here). We then extrapolated the potential contribution of the rest of the coccolithophore taxa using this factor (i.e., multiplying by 2.8 the *C. leptoporus* and minor species PIC values calculated in this study) (Fig. 7c). Both N-S coccolith mass and PIC trends mirror each other, but the C-Calcita-derived PICs tend to overestimate satellite-derived PIC values, except in a couple of locations. This can be attributed to the calibration of the coccolith thickness within the software C-Calcita, which has been improved in recent years with the use of a calcite wedge instead of a calcareous spine (e.g. Guitián et al., 2022).

The generally higher satellite-derived PIC numbers compared to the coccolith-estimated PIC values in the SAZ and PFZ (Figs. 3, 4, and 5S in Supplementary Material) could be also due to the presence of other carbonate-forming organisms (and/or their fragments); for instance, foraminifera, can contribute to a significant fraction of the total PIC in the SO south of Australia, especially between $55\text{--}60^\circ\text{S}$ (Trull et al., 2018). We do not have data for the Drake Passage, but planktonic foraminifera were observed in the filter samples across the New Zealand transect, showing increased abundance (together with the tintinnid species *Codonellopsis pusilla*) in the PFZ (see Malinverno et al., 2016 for further details). Although foraminifera and other hard-shelled micro-zooplankton PIC particles provide negligible backscatter per unit mass (Balch et al., 1996), they can be a

source of error in the PIC volume calculation when considering only coccolithophores. Assessing the significance of carbonate-forming organisms relative to other taxa in the SO is an important topic, but falls beyond the scope of this paper. -

Additionally, the fact that the difference between satellite PICs and in situ values in the Drake Passage transect is larger than in the New Zealand transect can be in part attributed to the fact that detached coccoliths (on top of coccospheres) were only considered in the estimates for the New Zealand transect.

Observed discrepancies between Part of the PIC- satellite-derived PIC and -coccolith-estimated estimate PIC values disparity can arise from a combination of several factors related to the PIC algorithm sensitivities and limitations (Mitchell et al., 2017; Balch and Mitchell, 2023; NASA Ocean Biology Processing Group, 2023), differences in time window -be attributed to the different-spatial and temporal resolutionseales- (Table 3), and environmental factors (e.g. turbidity or other particulate matter that can affect the accuracy of satellite-derived PIC estimates). MODIS-derived L2 PIC data- was limited due to the cloudy skies of the SO during the sampling period (see Figs. 1S and 2S in the Supplementary Material). oreed us to made it impossible to prevented us to use. match the the measurement time window and has similar time window expand the time window of the pixel extraction using -To mitigate the impact of these data gaps in our analysis, we extended the time window for data extraction to several days and computed the mean for each location, whilst also using L3 products. This approach, while necessary, could obscure potential variability at shorter temporal scales and create discrepancies when comparing with sample measurements taken onf specific days.

-However, the fact that the overall trends are comparable incomparable-incomparablethe same in in the New Zealand and Drake Passageis transects (Fig. 5S in the Supplementary Material), with values are different, -region and that in situ measurements agree with the remote sensing data, could also suggest that there is a satellite bias linked to the algorithm (which could be easily adjusted for the region north of the SO). We are aware that the MODIS-/Aqua Ocean Color was re-processed in 2022 (NASA Ocean Biology Processing Group, 2023a) to incorporate updates in instrument calibration, new ancillary sources and algorithm improvements (NASA Ocean Biology Processing Group, 2023a), but the validation of the PIC measurements wasis based just on a very-low number of in-situ measurements compared to other products (e.g.: 1347 in situ measurements for cChlorophyll a and just 42 for PIC, all of them in the Atlantic Ocean; NASA Ocean Biology Processing Group, 2023e, 2023b). -

The differences in PIC could also be due to the fact that we are comparing in situ values to weekly and monthly averages, as well as also smoothing data by considering averaged values when estimating coccolith-estimated PIC (especially length and number of coccoliths per coccosphere). In addition, sampling at slightly different times of the year may also have an influence on the PIC values determined (Rigual Hernández et al., 2018; Rigual-Hernández et al., 2020a, b).

In the study area, The SAZ and PFZ are generally characterized by moderate coccolithophore concentration with limited contribution from other biogenic particles (Figs. 3 and 4) (Malinverno et al., 2015; Malinverno et al., 2016; Saavedra-Pellitero et al., 2019). Given that *E. huxleyi* is the dominant species in both transects and the most important contributor to pelagic PIC,

Formatted: Font: (Default) Arial, 11 pt, Font color: Black

we focused on its abundance, morphotype distribution and calcite weight. Coccolith PIC calculated in this study for *E. huxleyi* are generally in agreement with the calcite content per coccolith obtained by Poulton et al. (2011) along the Patagonian Shelf and by Rigual Hernández et al. (2020a) in the Australian & New Zealand sectors of the SO (see Tables 1 in those papers). Our PIC *E. huxleyi* estimates seem generally higher than the estimates by Charalampopoulou et al. (2016) off southern Chile (0.015 pMol per coccolith) and across the rest of Drake Passage (< 0.009 pMol).

On the other hand, our values are slightly lower than those obtained through the birefringence method SYRACO, an automated system of coccolith recognition (SYstème de Reconnaissance Automatique de COccolithes) in the same latitudinal range (e.g. Beaufort et al., 2011) and notably lower than Saavedra Pellitero et al. (2019) across the Drake Passage using circularly polarised light plus the C-Calcita software developed by Fuertes et al. (2014) (Fig. 8a). In order to explore this difference, we calculated PICs in the Drake Passage using Saavedra Pellitero et al. (2019) mass estimates for the same samples, considering an average mass of 4.64 pMol for *E. huxleyi* ($n = 796$, standard deviation = 2.53) but without distinguishing different morphotypes (Fig. 8b). The mass per coccolith of *E. huxleyi* using C-Calcita in the Drake Passage is 2.8 times higher than in this work (mean of 1.66 pg in this work). We then used this factor to calculate the potential contribution of the rest of the coccolithophore taxa (see Figure 8). Both N-S coccolith mass and PIC trends mirror each other, but the C-Calcita-derived PICs tend to overestimate satellite values, except in a couple of locations. This can be attributed to the calibration of the coccolith thickness within the software C-Calcita, which has been improved in recent years with the use of a calcite wedge instead of a calcareous spine (e.g. Guitián et al., 2022). The differences in PIC could also be due to the fact that we are comparing in situ values to monthly averages, and also smoothing data by considering averaged values when estimating coccolith PICs (especially length and number of coccoliths per coccosphere). In addition, sampling at slightly different times of the year may also have an influence on the PIC values determined (Rigual Hernández et al., 2018; Rigual Hernández et al., 2020a, b). An increase in coccolith weight and size within morphotype B/C from December to August (but also from December to March) was observed at a sediment trap station deployed at 61°S in the Australian sector of the SO south of Tasmania (Rigual Hernández et al., 2018). Variations in light intensity in the mixed layer and increasing iron limitation were seen as the most likely drivers of this change. This could explain differences in the carbonate masses of different transects.

Our measurements on selected samples along the New Zealand transect, and across the Drake Passage show: (a) differences in calcification among the various *E. huxleyi* morphotypes, being very evident in type A (Figs. 3 b c, 4 b c, 5, and 67), (b) a wide scatter of relative tube width' within morphotypes and within each sample, especially marked in the New Zealand transect (Figs. 4b, 67) and (c) a slight decreasing trend in coccolith size and degree of calcification across the Drake Passage (Figs. 3b, 5a), which is not observed in the New Zealand transect. This suggests that environmental forcing does not significantly impact the degree of calcification but it clearly controls the distribution of *E. huxleyi* morphotypes (which are genetically based, Bendif et al., 2023) and thus indirectly impacts on the coccolith mass variation. This could also explain the southwards decreasing trend in calcification in the Drake Passage due to the fact that the relatively large and heavily calcified type A

eoecospheres are present in the northern SAZ and that. The PCA performed on the *E. huxleyi* morphometric dataset shows that those the heavily calcified type A eoecospheres occupy a relatively restricted ecological niche offshore of Chile (Fig. 67).

In general, we find a different pattern to that described in Balch et al. (2014), who determined coccolith-quotas in the center of a coccolithophore bloom in the Patagonian Shelf (Atlantic Ocean) ranging from 0.008 to 0.017 pg per coccolith by comparing automated coccolith-counts with coccolith-estimated in-situ PIC. In the context of other observations, the coccolith quotas calculated by Balch et al. (2014) are relatively low and show a much greater variation within a limited region. Considering the differences in the two SO transects studied here, which were sampled 11 years apart, we could assume that with our approach, the surface coccolith-estimated PIC calculations (up to 20 m water depth) do not underestimate underestimate actual-satellite-sea surface-derived PIC concentrations in the SAZ and PFZ. This is a likely possibility considering that coccolith PIC values using the same samples are higher than remote sensing PIC when calculated using a totally different methodology (for instance using C-Calcita). This discrepancy is evident in our data, whereas coccolith-estimated PIC concentrations calculated using different methodologies, such as C-Calcita, on our samples exceed those obtained from the satellite data. This indicates that there is still a need for improved precision in estimating coccolith-estimated PIC concentration methods. Therefore, it is crucial to refine existing methodologies and develop new algorithms to enhance accuracy. Additionally, the limited number of in situ data points used for calibrating satellite algorithms in the Southern Ocean (SO) could contribute to these discrepancies, highlighting the importance of expanding in situ datasets for better validation and calibration of remote sensing data. Nevertheless, an overestimation of the algorithm in the SO, due to the limited number of data points used for the calibration could also justify We attribute the discrepancy between the coccolithophore in-situ and satellite derived PIC values to overestimation of the algorithm in the SO, due to the limited number of data points used for the calibration.

5.2 Assessing potential biases in PIC estimates for the AZ

In the AZ (south of about 62.5°S in the New Zealand transect and about 60°S in the Drake Passage), high reflectance is detected by remote sensing but it is not associated with a coccolithophore bloom (Figs. 3, and 4 and S5). Concentrations of *E. huxleyi*, which show maximum numbers in the PFZ at the New Zealand transect and moderate values in the Drake Passage, drops southward of this location (Malinverno et al., 2016), at the Southern ACC Front and the PF (Malinverno et al., 2016).

Satellite data show the different impact of ACC fronts on the distribution of *E. huxleyi* (Holligan et al., 2010): in the Drake Passage, where the fronts are strictly constrained by topography, *E. huxleyi* is bounded by the PF to the south (Saavedra-

Pellitero et al., 2019), while in the eastern Scotia Sea, where the ACC fronts are broadly separated, *E. huxleyi* spreads between the PF and the Southern ACC Front (Holligan et al., 2010; Poulton et al., 2011; Poulton et al., 2013). This pattern also emerges from the compilation by Malinverno et al. (2016), which shows that the Southern ACC Front marks the southern boundary in different SOcean sectors.

Occasional occurrences of *E. huxleyi* south of the Southern ACC Front have been documented south of Tasmania and in the Weddell sea in certain years by conventional micropalaeontological observations (e.g. Winter et al., 1999; Cubillos et al., 2007) as well as in the Australian sector of the SO and in the Scotia Sea using surface reflectance data only (Holligan et al., 2010; Winter et al., 2014). However, in our this study present work, *E. huxleyi* is constrained by the Southern ACC Front corresponding to a maximum sea surface temperature of 1°C in the New Zealand transect.

The magnitude and spectral characteristics of water-leaving radiance detected by satellites are influenced by the inherent properties of the optically active constituents. These include: (1) light scattering by PIC, other biogenic particles or lithogenic material (e.g. Bi et al., 2023) as well as (2) light absorption by phytoplankton biomass (i.e., chlorophyll *a* concentration) and dissolved organic matter (e.g. Reynolds et al., 2001; Ferreira et al., 2009). The strong correlation between high values of water-leaving radiance and high *E. huxleyi* PIC concentrations has been successfully proved in bloom areas (e.g. Gordon et al., 1988; Balch et al., 2005; Holligan et al., 2010; Balch et al., 2011; Balch et al., 2014; Balch and Mitchell, 2023; Oliver et al., in press 2023). However, not all bright waters are caused by *E. huxleyi* blooms, as shown by Broerse et al. (2003) in the Bering Sea, Balch et al. (2007) in the Gulf of Maine, and Daniels et al. (2012) in the Bay of Biscay. Suspended particles, which include either reworked coccoliths, lithogenic material or empty diatom frustules, could be responsible for high values of water-leaving radiance, at least in nearshore regions (Broerse et al., 2003; Balch and Mitchell, 2023).

The occurrence of bright waters along the studied transects should theoretically be constrained by the position of the PF/Southern ACC Front. Malinverno et al. (2015; 2016) showed a significant shift in the community composition from carbonate to silica-dominated microfossils in the New Zealand transect at the Southern ACC Front, with diatoms being the most abundant mineralized phytoplankton group in the transect (Fig. 3k). Coccolithophores disappear south of the Southern ACC Front, and the composition of the siliceous phytoplankton changes from a dominance of large diatoms (*Fragilariopsis kerguelensis*) in the north to a dominance of small diatoms (such as the cold adapted *Fragilariopsis cylindrus*) in the south, with a notable increase in spiny silicoflagellates (e.g., *Stephanocha speculum* var. *coronata*) and small siliceous plankton (Parmales, Archaeomonads) (Malinverno et al., 2016) coincident with high values of chlorophyll *a* in the AZ (Figs. 3l, 89). The extant diatoms present have not yet been studied in the exact same water samples collected during PS97 Expedition. However, the abundance of subfossil diatoms in surface sediments in the Drake Passage shows an increase south of the PF, along with an increase in the relative abundance of siliciclastics, -biogenic opal (Cárdenas et al., 2018). This contrasts with the relatively low satellite-derived chlorophyll *a* concentration in the AZ (Fig. 4k), but this only due to the very limited number of daily L2 data

620 available. *Fragilariopsis kerguelensis* appears to dominate up to the Southern ACC Front, and *F. cylindrus* is found south of
621 this front, in colder waters of the Drake Passage (Cárdenas et al., 2018).

622
623 Different alternatives have been suggested in the literature for the high reflectance in the AZ of the SO, such as microbubbles
624 (mostly during storms), floating loose ice, high concentrations of other particulate matter such as glacial flour (especially close
625 to the Antarctic continent) or Phaeocystis blooms (Balch et al., 2011; Balch, 2018; Balch and Mitchell, 2023). However,
626 considering our approach, does not allow us we would have not been able to visualize soft-bodied Phaeocystis, ice crystals or
627 bubbles, even if they were initially present. Our observations do not allow us to comprehensively determine the potential
628 causes of this high reflectance. Based on our observations, and even though opal particles have a much lower refractive index
629 than calcite (Balch, 2009; Costello et al., 1995), but we note we suggest that the high abundance of small opal biogenic
630 particles, such as small-size diatoms, silicoflagellates and siliceous plankton observed (as well as their fragments) would be
631 consistent with could explain the observed high scattering of these waters at least in the New Zealand transect (Figs. 1, 3, 4, 3S
632 and 4S in Supplementary Material), even though opal particles have a much lower refractive index than calcite (Balch, 2009;
633 Costello et al., 1995).

634
635 Although opal particles have a much lower refractive index than calcite (Balch, 2009; Costello et al., 1995), we suggest that
636 the high abundance of small opal particles observed could explain the observed high scattering of these waters at least
637 in the New Zealand transect (Figs. 1, 3, 4). Alternative sources of high reflectance in the SO considered by other authors
638 include microbubbles (mostly during storms), floating loose ice or high concentrations of other particulate matter such as
639 glacial flour (especially close to the Antarctic continent) or Phaeocystis blooms (Balch et al., 2011; Balch, 2018; Balch and
640 Mitchell, 2023).

642 5.3 *Emiliania huxleyi* morphotypes

643 The PCA performed on the *Emiliania huxleyi* morphometric dataset in particular reveals that a Type A overcalcified
644 morphotype that is highly distinct from the other morphotypes (Fig. 6). This morphotype has also been previously observed in
645 the coastal waters of the eastern South Pacific and in the open ocean (Beaufort et al., 2011; Von Dassow et al., 2018; Saavedra-
646 Pellitero et al., 2019). However, it should be noted that type A overcalcified in this work includes the moderately calcified,
647 robustly calcified and extremely heavily calcified A morphotypes described by Diaz-Rosas et al. (2021). Coccospheres of *E.*
648 *huxleyi* classified by Diaz-Rosas et al. (2021) as extremely heavily calcified R/hyper-calcified and/or A-CC morphotypes (with
649 complete overgrowth of the coccolith central area but without fusion of distal shield elements) occasionally occurred offshore
650 of Chile in samples closest to the coastline (see an example in Fig. 6). In the Southern Hemisphere, these extremely heavily
651 calcified morphotypes were only previously observed at the Pacific border of southern Patagonia (in the Archipelago Madre
652 de Dios Fjord area) and in the Northern Hemisphere, in Norwegian fjords (e.g. Young et al., 2014). Diaz-Rosas et al. (2021)
653 suggested that the R/hyper-calcified morphotype has a marginal ecological niche preference compared to moderately calcified

Formatted: Normal

Formatted: Font: Bold

Formatted: Font: Bold

Formatted: Font: Bold

types A and A-CC. Therefore, the few specimens of *E. huxleyi* type A overcalcified (i.e. heavily calcified looking in between the R/hyper-calcified and/or A-CC morphotypes by Diaz-Rosas et al. (2021)) observed in this work, and by Saavedra-Pellitero et al. (2019) in the Drake Passage, could be attributed to different niches overlapping offshore of Chile.

The normal type A specimens show a moderate range of variation in tube width, comparable to type O, but smaller than B, B/C-C, with type C having the thinnest tube width. The distal shield element width and the number of T-elements of the different specimens are closely related to the length and width measured (Fig. 67) as they are all indicators of coccolith size. There is broader variation in coccolith size (length and width) within morphogroup B compared to morphogroup A, which is more restricted. Suchéras-Marx et al (2022) pointed out that *E. huxleyi* coccolith size is limited by the cell diameter because heterococcoliths are produced intracellularly and are extruded later on. Interestingly, specimens of *E. huxleyi* type A in the New Zealand transect are notably smaller than those offshore of Chile, which we link to local adaptations, seasonality and even ecological interactions such as predation (e.g. Monteiro et al., 2016; Hansen et al., 1996).

However, the coccolithophore assemblages in the PFZ and south of it are monospecific, which is also known from other areas of the SO (e.g. Charalampopoulou et al., 2016), and consist almost entirely of *E. huxleyi* morphogroup B. The mean placolith length of *E. huxleyi* morphogroup B (including types B, B/C-C, and O) in both transects is very similar (Drake Passage: $2.98 \pm 0.40 \mu\text{m}$, New Zealand: $2.87 \pm 0.35 \mu\text{m}$) and agrees well with the corresponding B/C measurements of Charalampopoulou et al. (2016) in samples retrieved in 2009 in the Drake Passage (2.8 μm). Still, our averaged values are slightly lower than the mean length estimated by Poulton et al. (2011) on the Patagonian Shelf ($3.25 \pm 0.40 \mu\text{m}$). This could be due to the fact that Poulton et al. (2011) did not distinguish between types B and O (i.e. they were merged into B/C), which are typically larger coccoliths than B/C (Fig. 6) and could have contributed to increase the averaged length. The length range for types B/C-C (Drake Passage: 2.20 to $3.98 \pm 0.37 \mu\text{m}$, New Zealand: 1.95 to $3.62 \pm 0.33 \mu\text{m}$) agrees quite well with the range reported by Cook et al. (2011) for cultured B/C strains (2.65 to 4.80 μm) and is in the range of sizes presented by Charalampopoulou et al. (2016) for the Drake Passage (1.8 to 5.5 μm). The fact that we record lower values is simply a matter of taxonomical considerations regarding the overlapping sizes of morphotypes B, B/C, C and O, visually represented in Figure 6.

Overall, our morphometric data from selected samples along the New Zealand transect, and across the Drake Passage transects show: (1a) differences in calcification between among the different various *E. huxleyi* morphotypes, which are particularly being very evident in type A (Figs. 3, 4, 5, and 6), (2b) a large wide scatter of relative tube width within morphotypes and within each sample, particularly pronounced especially marked in the New Zealand transect (Figs. 4, 6), and (3e) a slight decreasing trend in coccolith size and degree of calcification in across the Drake Passage (Figs. 3, 6), which is not observed in the New Zealand transect. This suggests that environmental influences foreign have does no t-significantly effect on impact the degree of calcification, but it clearly controls the distribution of *E. huxleyi* morphotypes (which are genetically-

determined based on Bendif et al., 2023) and thus indirectly affects the coccolith mass variation. This could also explain the southwards decreasing trend in calcification in the Drake Passage, as due to the fact that the relatively large and heavily calcified type A coccospheres occur are present in the northern SAZ

The different taxonomic considerations of *E. huxleyi* in different studies make it difficult to compare and combine data, especially in light of recent advances in the field. Given the dominance of this taxa in the SO, a key area for global warming and ocean acidification studies, the efforts by the scientific nanofloral community should focus on a more uniform classification of *E. huxleyi* morphotypes. However, differentiation and recognition of the various morphotypes is time consuming and tedious and plays only a minor role in the calculation of the total coccolithophore PIC, as observed in other areas of the SO (e.g. Rigual Hernández et al., 2020a, b). The changes in masses within the B morphotype (with types B/C-C, C, O) in the two transects are negligible in the PIC calculation, while a differentiation into morphogroups A and B has an influence on the calculation of the PIC. However, specimens of *E. huxleyi* belonging to morphogroup A only occur in the northern areas of both transects, where they play a role together with the PIC input from other massive species such as *C. leptoporus* (Fig. 5). Overall, the changes in total coccolithophore-PIC in the study area are caused by the abundance and occurrence within the entire coccolithophore community. The relative contribution of the different *E. huxleyi* morphogroups to the coccolithophore-PIC in the SO deserves further exploration in light of the rapid development of remote sensing algorithms and recent evolution of machine learning approaches for PIC estimates.

6 Conclusions/Summary

The comparison between particulate inorganic carbon (PIC) derived from satellite data and in situ coccolithophore-based estimates in two transects of the Pacific sector (separated in time and space) demonstrates provides awareness of the limited availability of high-quality PIC-satellite-derived data (mostly due to atmospheric conditions), and the need for refining methodologies to accurately produce estimate-coccolith-estimated PIC. , so it is important to refine methodologies in the future to improve accuracy

-an invaluable ground-truth benchmark for the study of coccolithophores at high latitudes. Based on our data the following conclusions can be drawn:

- 1) We found out that satellite-derived PIC values and coccolith-estimated derived PIC values trends follow a comparable trend are in good agreement in the Subantarctic Zone (SAZ) and Polar Front Zone (PFZ). However, satellite-derived PIC values are generally higher than coccolith-estimated derived PIC. This difference could be due to a lack in precision in the coccolith-based PIC estimates, to the presence of foraminifera and/or other hard-shelled micro-zooplankton adding potential error when calculating total PIC volume, or to a remote sensing tends to

overestimate PIC values, which we link to a certain bias in the algorithm due to the ~~low~~limited number of measurements used for the validation of the ~~satellite-derived~~ PIC calibration (all of ~~which were taken~~ them in the Atlantic Ocean). ~~This could be potentially adjusted for in the Southern Ocean and specifically for the study area.~~

2) ~~There is an A striking observation is the~~observed decoupling of satellite-derived PIC and ~~coccolith-estimated~~coccolith-estimated PIC estimates ~~at and to the~~south of the Polar Front (PF), ~~particularly~~in the Antarctic Zone (AZ). Despite having ~~satellite~~ high reflectance values, no coccolithophores were observed in this area ~~of high chlorophyll a concentration~~. We ~~are unable to determine the reason for this with our data, but note~~hypothesize that ~~the high satellite-derived PIC values in the AZ are consistent with~~ could be due to the ~~high~~ ~~the an~~ abundance of ~~small biogenic opal particles, such as small-size diatoms, silicoflagellates and/or siliceous plankton (as well as their fragments) small opal particles or, as suggested by other authors, potential other biogenic particles not visible in scanning electron microscope (e.g. SEM. Phaeocystis aggregations, microbubbles, etc.) could possibly provide an explanation for this observation.~~

3) *Emiliana huxleyi* is the predominant coccolithophore species contributing the most to the ~~total~~ sea-surface ~~coccolith-~~PIC in the New Zealand transect (mainly sampled in 2005) and as well as in the Drake Passage (sampled in 2016). *Calcidiscus leptoporus* may occasionally contribute significantly to the ~~total coccolithophore-PIC~~ ~~contributions~~ at certain locations, whereas the rest of the coccolithophore taxa contribute only marginally ~~to the PIC~~ in the studied areas.

4) *Emiliana huxleyi* consists of ~~several~~different morphotypes, which have different, partly overlapping geographical distributions. The relatively massive ~~t~~Type A occurs in the northern SAZ and occasionally in the PFZ of the Drake Passage, while specimens of the less calcified morphogroup B (which includes ~~t~~Types B, B/C, C and O) occur in the SAZ and the PFZ of both transects, but disappear drastically south of the PF. But neither the slightly different carbonate masses nor the southward changes in morphotype composition have a decisive influence on the coccolith~~ophore-estimated~~derived PIC, which is only determined by the ~~abundance~~amount of *E. huxleyi* in this area.

5) ~~The satellite-derived and coccolith-estimated~~based PIC discrepancies ~~we~~observed in this work emphasizes the importance of in situ measurements ~~and sampling; it also~~and highlights the need for further investigation to fully understand the factors influencing water-leaving radiance and the reliability of remote sensing estimates, especially south of the PF.

Future research should focus on refining ~~methodologies~~ and -satellite algorithms to improve the accuracy of PIC estimates and better understand the dynamics of coccolithophores ~~communities~~as well ~~generally~~ phytoplankton and zooplankton ~~communities~~ in the Pacific sector of the Southern Ocean (especially compared to ~~other~~the Atlantic and Indian sectors). Such

Formatted: No bullets or numbering

Formatted: Font: (Default) Arial, 11 pt, Font color: Black

754 efforts will enhance our understanding of carbon cycling and its impact on marine ecosystems ~~at in this key~~ high latitudes
755 ~~region~~.

756 Acknowledgements

757 Satellite-derived Particulate Inorganic Carbon (PIC) data ~~was downloaded~~~~was were downloaded~~ from the Ocean_Color Web
758 Level ~~1 & 2~~ Browser (<https://oceancolor.gsfc.nasa.gov/cgi/browse.pl?sen>) and ~~2~~ Level ~~3~~ & 4 Browser
759 (<https://oceancolor.gsfc.nasa.gov/l3>), ~~a both of them~~ services provided by NASA's Ocean Biology Distributed Active Archive
760 Centre ([OB.DAAC](#)).

761 The authors acknowledge the use of the JASMIN (Joint Analysis System for the Met Office, NERC, and UKRI)
762 (<https://jasmin.ac.uk/>) Jupyter Notebook service to process the ~~satellite-derived~~ PIC data. We would like to express our
763 gratitude to the JASMIN team for their support and the valuable resources they provide to the scientific community.

764 ~~The authors are grateful to two anonymous reviewers and to the handling associate editor, Prof. Shutler, for their invaluable~~
765 ~~suggestions on a previous version of the paper.~~ The Alfred Wegener Institute Bremerhaven provided part of the plankton
766 samples required for this study. Frank Lamy, Hartmut Schulz, ~~R/V Polarstern~~ ~~OLARSTERN~~ officers and crew are thanked for
767 their help during the PS97 Expedition.

768 Dr. Frigola (Barcelona Supercomputing Center, Spain), Dr. Merkel (University of Bremen/MARUM, Germany) and Dr.
769 Hardiman (University of Portsmouth, UK) are acknowledged for their help with remote sensing data collection ~~advice~~. Dr.
770 Pepin (University of Portsmouth, UK) and Dr. Balch (Bigelow Laboratory for Ocean Sciences, USA) are thanked for their
771 comments and suggestions on this piece of research during the "Advances in Coccolithophore research" meeting. Dr. Saavedra
772 (RIP) is thanked for his continuous encouragement to finish up this paper.

773 Financial support

774 This research was supported by University of Portsmouth, ~~and by the~~ Deutsche Forschungsgemeinschaft ~~Adaptation of~~
775 ~~cooccolithophore communities to environmental change in the Southern Ocean (no. BA 1648/30-1) with a grant~~ to Karl-Heinz
776 Baumann (reference number: BA 1648/30-1), ~~contributed with through~~ previous funding for Mariem Saavedra-Pellitero and
777 Nele M. Vollmar, ~~as well as and by~~ the MIUR project "Dipartimenti di Eccellenza 2018/2023" for Elisa Malinverno, at
778 the Department of Earth and Environmental Sciences, University of Milano-Bicocca. ~~The University of Portsmouth Research~~
779 ~~and Innovation Services, as well as Copernicus Publications are acknowledged for their additional financial support to publish~~
780 ~~this paper as Open Access.~~

782 Data Availability Statement

Formatted: Font: Italic

Formatted: Font: Italic

783 The authors confirm that the data from which the findings of this study are available within the article Supplementary Materials
784 and are stored in the data repository <https://pangaea.de/> (<https://doi.pangaea.de/10.1594/PANGAEA.964672>
785 and <https://doi.pangaea.de/10.1594/PANGAEA.964674>)
786

787 **Author contributions**

788 The study was designed by EM, MSP and KHB. EM and NMV carried out the morphometric measurements and classified the
789 specimens of *E. huxleyi*. EM and MSP calculated coccolith-PICs, plotted the data and wrote an earlier version of the
790 manuscript. N-B-J and HL provided remote sensing data for the study area, and were actively involved in the discussion of the
791 findings as well as in the writing of the paper. All authors approved the submitted version.

792 **References**

- 793 Babin, M., Morel, A., Fournier-Sicre, V., Fell, F., and Stramski, D.: Light scattering properties of marine particles in coastal
794 and open ocean waters as related to the particle mass concentration, *Limnology and Oceanography*, 48, 843-859, doi:
795 10.4319/lo.2003.48.2.0843, 2003a.
- 796 Babin, M., Stramski, D., Ferrari, G. M., Claustre, H., Bricaud, A., Obolensky, G., and Hoepffner, N.: Variations in the light
797 absorption coefficients of phytoplankton, nonalgal particles, and dissolved organic matter in coastal waters around
798 Europe, *Journal of Geophysical Research: Oceans*, 108, doi: 10.1029/2001JC000882, 2003b.
- 799 [Bailey, S. W., & Werdell, P. J. \(2006\). A multi-sensor approach for the on-orbit validation of ocean color satellite data products.](#)
800 [Rem. Sens. Environ., 102, 12-23.](#)
- 801 Balch, W. M.: The Ecology, Biogeochemistry, and Optical Properties of Coccolithophores, *Annual Review of Marine Science*,
802 10, 71-98, doi: 10.1146/annurev-marine-121916-063319, 2018.
- 803 Balch, W. M., Holligan, P. M., Ackleson, S. G., and Voss, K. J.: Biological and optical properties of mesoscale coccolithophore
804 blooms in the Gulf of Maine, *Limnology and Oceanography*, 36, 629-643, doi: 10.4319/lo.1991.36.4.0629, 1991.
- 805 Balch, W. M., Kilpatrick, K. A., Holligan, P., Harbour, D., and Fernandez, E.: The 1991 coccolithophore bloom in the central
806 North Atlantic. 2. Relating optics to coccolith concentration, *Limnology and Oceanography*, 41, 1684-1696, 1996.
- 807 Balch, W. M., Drapeau, D. T., Cucci, T. L., Vaillancourt, R. D., Kilpatrick, K. A., and Fritz, J. J.: Optical backscattering by
808 calcifying algae: Separating the contribution of particulate inorganic and organic carbon fractions, *Journal of Geophysical*
809 *Research: Oceans*, 104, 1541-1558, doi: 10.1029/1998JC900035, 1999.
- 810 Balch, W. M., Gordon, H. R., Bowler, B. C., Drapeau, D. T., and Booth, E. S.: Calcium carbonate measurements in the surface
811 global ocean based on Moderate-Resolution Imaging Spectroradiometer data, *Journal of Geophysical Research: Oceans*,
812 110, doi: 10.1029/2004JC002560, 2005.

813 Balch, W. M., Drapeau, D. T., Bowler, B. C., Booth, E. S., Windecker, L. A., and Ashe, A.: Space–time variability of carbon
814 standing stocks and fixation rates in the Gulf of Maine, along the GNATS transect between Portland, ME, USA, and
815 Yarmouth, Nova Scotia, Canada, *Journal of Plankton Research*, 30, 119–139, doi: 10.1093/plankt/fbm097, 2007.

816 Balch, W. M., Drapeau, D. T., Bowler, B. C., Lyczkowski, E., Booth, E. S., and Alley, D.: The contribution of
817 coccolithophores to the optical and inorganic carbon budgets during the Southern Ocean Gas Exchange Experiment: New
818 evidence in support of the “Great Calcite Belt” hypothesis, *Journal of Geophysical Research: Oceans*, 116, doi:
819 10.1029/2011jc006941, 2011.

820 Balch, W. M., Drapeau, D. T., Bowler, B. C., Lyczkowski, E. R., Lubelczyk, L. C., Painter, S. C., and Poulton, A. J.: Surface
821 biological, chemical, and optical properties of the Patagonian Shelf coccolithophore bloom, the brightest waters of the
822 Great Calcite Belt, *Limnology and Oceanography*, 59, 1715–1732, doi: 10.4319/lo.2014.59.5.1715, 2014.

823 Balch, W. M., Bates, N. R., Lam, P. J., Twining, B. S., Rosengard, S. Z., Bowler, B. C., Drapeau, D. T., Garley, R., Lubelczyk,
824 L. C., Mitchell, C., and Rauschenberg, S.: Factors regulating the Great Calcite Belt in the Southern Ocean and its
825 biogeochemical significance, *Global Biogeochemical Cycles*, 30, 1124–1144, doi: 10.1002/2016gb005414, 2016.

826 Balch, W. M., and Mitchell, C.: Remote sensing algorithms for particulate inorganic carbon (PIC) and the global cycle of PIC,
827 *Earth-Science Reviews*, 239, 104363, doi: 10.1016/j.earscirev.2023.104363, 2023.

828 Balch, W. M., and P.E. Utgoff: Potential interactions among ocean acidification, coccolithophores, and the optical properties
829 of seawater, *Oceanography and Marine Biology Annual Review*, 22, 146–159, doi: 10.5670/oceanog.2009.104, 2009.

830 [Baumann, K.-H.: Importance of coccolith size measurements for carbonate estimations. *Micropaleontology*, 50 \(1\), 35–43, 2004.](#)

831

832 Beaufort, L.: Weight estimates of coccoliths using the optical properties (birefringence) of calcite, *Micropaleontology*, 51,
833 289–298, 2005.

834 Beaufort, L., Probert, I., de Garidel-Thoron, T., Bendif, E. M., Ruiz-Pino, D., Metzl, N., Goyet, C., Buchet, N., Coupel, P.,
835 Grelaud, M., Rost, B., Rickaby, R. E. M., and de Vargas, C.: Sensitivity of coccolithophores to carbonate chemistry and
836 ocean acidification, *Nature*, 476, 80–83, doi: 10.1038/nature10295, 2011.

837 Bendif, E. M., Probert, I., Archontikis, O. A., Young, J. R., Beaufort, L., Rickaby, R. E., and Filatov, D.: Rapid diversification
838 underlying the global dominance of a cosmopolitan phytoplankton, *The ISME Journal*, 17, 630–640, doi: 10.1038/s41396-
839 023-01365-5, 2023.

840 Beuvier, T., Probert, I., Beaufort, L., Suchéras-Marx, B., Chushkin, Y., Zontone, F., and Gibaud, A.: X-ray nanotomography
841 of coccolithophores reveals that coccolith mass and segment number correlate with grid size, *Nature Communications*,
842 10, 751, doi: 10.1038/s41467-019-08635-x, 2019.

843 [Bevington, P. R., *Data Reduction and Error Analysis for the Physical Sciences*, 336 pp., McGraw-Hill, 1969](#)

844

845 Bi, S., Hieronymi, M., and Röttgers, R.: Bio-geo-optical modelling of natural waters, *Frontiers in Marine Science*, 10, doi:
846 10.3389/fmars.2023.1196352, 2023.

847 Bollmann, J.: Technical Note: Weight approximation of coccoliths using a circular polarizer and interference colour derived
848 retardation estimates - (The CPR Method), *Biogeosciences*, 11, 1899-1910, doi: 10.5194/bg-11-1899-2014, 2014.

849 Broerse, A. T. C., Tyrrell, T., Young, J. R., Poulton, A. J., Merico, A., Balch, W. M., and Miller, P. I.: The cause of bright
850 waters in the Bering Sea in winter, *Continental Shelf Research*, 23, 1579-1596, doi: 10.1016/j.csr.2003.07.001, 2003.

851 Cárdenas, P., Lange, C. B., Vernet, M., Esper, O., Strain, B., Vorrath, M.-E., Ehrhardt, S., Müller, J., Kuhn, G., Arz, H. W.,
852 Lembke-Jene, L., and Lamy, F.: Biogeochemical proxies and diatoms in surface sediments across the Drake Passage
853 reflect oceanic domains and frontal systems in the region, *Progress in Oceanography*, doi: 10.1016/j.pocean.2018.10.004,
854 2018.

855 Charalampopoulou, A., Poulton, A. J., Bakker, D. C. E., Lucas, M. I., Stinchcombe, M. C., and Tyrrell, T.: Environmental
856 drivers of coccolithophore abundance and calcification across Drake Passage (Southern Ocean), *Biogeosciences*, 13,
857 5917-5935, doi:10.5194/bg-13-5917-2016, 2016.

858 Cook, S. S., Whittock, L., Wright, S. W., and Hallegraeff, G. M.: Photosynthetic pigment and genetic differences between two
859 Southern Ocean morphotypes of *Emiliana huxleyi* (Haptophyta), *Journal of Phycology*, 47, 615-626, doi:
860 10.1111/j.1529-8817.2011.00992.x, 2011.

861 Costello, D. K., Carder, K. L., and Hou, W.: Aggregation of diatom bloom in a mesocosm: Bulk and individual particle optical
862 measurements, *Deep Sea Research Part II: Topical Studies in Oceanography*, 42, 29-45, doi: 10.1016/0967-
863 0645(95)00003-9, 1995.

864 Cros, L., Kleijne, A., Zeltner, A., Billard, C., and Young, J. R.: New examples of holococcolith-heterococcolith combination
865 coccospheres and their implications for coccolithophorid biology, *Marine Micropaleontology*, 39, 1-34, doi:
866 10.1016/S0377-8398(00)00010-4, 2000.

867 Cubillos, J. C., Wright, S. W., Nash, G., de Salas, M. F., Griffiths, B., Tilbrook, B., Poisson, A., and Hallegraeff, G. M.:
868 Calcification morphotypes of the coccolithophorid *Emiliana huxleyi* in the Southern Ocean: changes in 2001 to 2006
869 compared to historical data, *Marine Ecology Progress Series*, 348, 47-54, doi: 10.3354/meps07058, 2007.

870 Daniels, C. J., Tyrrell, T., Poulton, A. J., and Pettit, L.: The influence of lithogenic material on particulate inorganic carbon
871 measurements of coccolithophores in the Bay of Biscay, *Limnology and Oceanography*, 57, 145-153, doi:
872 10.4319/lo.2012.57.1.0145, 2012.

873 [Davis, J. C.: Statistics and Data Analysis in Geology, John Wiley & Sons, 1986.](#)

874 de Baar, H. J. W., de Jong, J. T. M., Bakker, D. C. E., Loscher, B. M., Veth, C., Bathmann, U., and Smetacek, V.: Importance
875 of iron for plankton blooms and carbon dioxide drawdown in the Southern Ocean, *Nature*, 373, 412-415, doi:
876 10.1038/373412a0, 1995.

877 Devred, E., Sathyendranath, S., Stuart, V., Maass, H., Ulloa, O., and Platt, T.: A two-component model of phytoplankton
878 absorption in the open ocean: Theory and applications, *Journal of Geophysical Research: Oceans*, 111, doi:
879 10.1029/2005JC002880, 2006.

880 Díaz-Rosas, F., Alves-de-Souza, C., Alarcón, E., Menschel, E., González, H. E., Torres, R., and von Dassow, P.: Abundances
 881 and morphotypes of the coccolithophore *Emiliana huxleyi* in southern Patagonia compared to neighbouring oceans and
 882 Northern Hemisphere fjords, *Biogeosciences*, 18, 5465-5489, doi: 10.5194/bg-18-5465-2021, 2021.
 883 Ferreira, A., Garcia, V. M. T., and Garcia, C. A. E.: Light absorption by phytoplankton, non-algal particles and dissolved
 884 organic matter at the Patagonia shelf-break in spring and summer, *Deep Sea Research Part I: Oceanographic Research*
 885 *Papers*, 56, 2162-2174, doi: 10.1016/j.dsr.2009.08.002, 2009.
 886 Fuertes, M.-Á., Flores, J.-A., and Sierro, F. J.: The use of circularly polarized light for biometry, identification and estimation
 887 of mass of coccoliths, *Marine Micropaleontology*, 113, 44-55, doi: 10.1016/j.marmicro.2014.08.007, 2014.
 888 GEBCO Compilation Group: GEBCO_2022 Grid. Data set available online from the British Oceanographic Data Centre,
 889 Liverpool, UK. doi: 10.5285/e0f0bb80-ab44-2739-e053-6c86abc0289c, 2022.
 890 Gordon, A. L., Molinelli, E., and Baker, T.: Large-scale relative dynamic topography of the Southern Ocean, *Journal of*
 891 *Geophysical Research: Oceans*, 83, 3023-3032, doi: 10.1029/JC083iC06p03023, 1978.
 892 Gordon, H. R., Brown, O. B., Evans, R. H., Brown, J. W., Smith, R. C., Baker, K. S., and Clark, D. K.: A semianalytic radiance
 893 model of ocean color, *Journal of Geophysical Research: Atmospheres*, 93, 10909-10924, doi:
 894 10.1029/JD093iD09p10909, 1988.
 895 Gordon, H. R., Boynton, G. C., Balch, W. M., Groom, S. B., Harbour, D. S., and Smyth, T. J.: Retrieval of coccolithophore
 896 calcite concentration from SeaWiFS Imagery, *Geophysical Research Letters*, 28, 1587-1590, doi:
 897 10.1029/2000GL012025, 2001.
 898 Gravalosa, J. M., Flores, J.-A., Sierro, F. J., and Gersonde, R.: Sea surface distribution of coccolithophores in the eastern
 899 Pacific sector of the Southern Ocean (Bellingshausen and Amundsen Seas) during the late austral summer of 2001,
 900 *Marine Micropaleontology*, 69, 16-25, doi: 10.1016/j.marmicro.2007.11.006, 2008.
 901 Guitián, J., Fuertes, M. Á., Flores, J. A., Hernández-Almeida, I., and Stoll, H.: Variation in calcification of Reticulofenestra
 902 coccoliths over the Oligocene–Early Miocene, *Biogeosciences*, 19, 5007-5019, doi: 10.5194/bg-19-5007-2022, 2022.
 903 ~~Oliver, H., McGillicuddy, D. J., J., Krumhardt, K. M., Long, M. C., Bates, N. R., Bowler, B. C., Drapeau, D. T., and Balch,~~
 904 ~~W. M.: Environmental drivers of coccolithophore growth in the Pacific sector of the Southern Ocean, *Global*~~
 905 ~~*Biogeochemical Cycles*, in press.~~
 906 ~~Hammer, Ø., Harper, D. A. T., and Ryan, P. D.: PAST: paleontological Statistics software package for education and data~~
 907 ~~analysis, *Paleontologia Electronica*, 49, 9, 2001.~~
 908 Hansen, F. C., Witte, H. J., and Passarge, J.: Grazing in the heterotrophic dinoflagellate *Oxyrrhis marina*: Size selectivity and
 909 preference for calcified *Emiliana huxleyi* cells., *Aquatic Microbial Biology*, 10, 307–313, 1996.
 910 Harlay, J., Borges, A. V., Van Der Zee, C., Delille, B., Godoi, R. H. M., Schiettecatte, L. S., Roelvros, N., Aerts, K., Lapernat,
 911 P. E., Rebreanu, L., Groom, S., Daro, M. H., Van Grieken, R., and Chou, L.: Biogeochemical study of a coccolithophore
 912 bloom in the northern Bay of Biscay (NE Atlantic Ocean) in June 2004, *Progress in Oceanography*, 86, 317-336, doi:
 913 10.1016/j.pocean.2010.04.029, 2010.

914 Harper, D. A. T.: Numerical Palaeobiology, John Wiley & Sons, 1999.

915 Holligan, P. M., Viollier, M., Harbour, D. S., Camus, P., and Champagne-Philippe, M.: Satellite and ship studies of
 916 coccolithophore production along a continental shelf edge, *Nature*, 304, 339-342, doi: 10.1038/304339a0, 1983.

917 ~~Holligan, P. M., Fernández, E., Aiken, J., Balch, W. M., Boyd, P., Burkill, P. H., Finch, M., Groom, S. B., Malin, G., Muller,~~
 918 ~~K., Purdie, D. A., Robinson, C., Trees, C. C., Turner, S. M., and van der Wal, P.: et al. (1993). A biogeochemical study~~
 919 ~~of the coccolithophore, *Emiliana huxleyi*, in the~~
 920 ~~north Atlantic. *Global Biogeochem. Cycles*, 7(4), 879-900. A biogeochemical study of the coccolithophore, *Emiliana huxleyi*,~~
 921 ~~in the North Atlantic. *Global Biogeochemical Cycles*, 7, 879-900, doi: 10.1029/93gb01731, 1993.~~

922 Holligan, P. M., Charalampopoulou, A., and Hutson, R.: Seasonal distributions of the coccolithophore, *Emiliana huxleyi*, and
 923 of particulate inorganic carbon in surface waters of the Scotia Sea, *Journal of Marine Systems*, 82, 195-205, doi:
 924 10.1016/j.jmarsys.2010.05.007, 2010.

925 Horigome, M. T., Ziveri, P., Grelaud, M., Baumann, K. H., Marino, G., and Mortyn, P. G.: Environmental controls on the
 926 *Emiliana huxleyi* calcite mass, *Biogeosciences*, 11, 2295-2308, doi: 10.5194/bg-11-2295-2014, 2014.

927 Iida, T., Saitoh, S. I., Miyamura, T., Toratani, M., Fukushima, H., and Shiga, N.: Temporal and spatial variability of
 928 coccolithophore blooms in the eastern Bering Sea, 1998-2001, *Progress in Oceanography*, 55, 165-175, doi:
 929 10.1016/S0079-6611(02)00076-9, 2002.

930 Kleijne, A.: Morphology, taxonomy and distribution of extant coccolithophores (calcareous nannoplankton), Ph.D., Vrije
 931 Universiteit, Amsterdam, 321 pp., 1993.

932 Klinck, J., and Nowlin, W. D.: Antarctic Circumpolar Current, in: *Encyclopedia of Ocean Sciences*, edited by: Steele, J. H.,
 933 Academic Press, Oxford, 151-159, 2001.

934 Krumhardt, K. M., Lovenduski, N. S., Long, M. C., Levy, M., Lindsay, K., Moore, J. K., and Nissen, C.: Coccolithophore
 935 growth and calcification in an acidified ocean: Insights from Community Earth System Model simulations, *Journal of*
 936 *Advances in Modeling Earth Systems*, doi: 10.1029/2018ms001483, 2019.

937 Lamy, F.: The Expedition PS97 of the Research Vessel POLARSTERN to the Drake Passage in 2016, edited by: Berichte zur
 938 Polar- und Meeresforschung = Reports on polar and marine research, E. b. F. L. w. c. o. t. p., 167 pp., 2016.

939 ~~Legendre, P., and Legendre, L.: Numerical Ecology, 2nd ed., Elsevier, 1998.~~

940 Malinverno, E., Triantaphyllou, M. V., and Dimiza, M. D.: Coccolithophore assemblage distribution along a temperate to polar
 941 gradient in the West Pacific sector of the Southern Ocean (January 2005) *Micropaleontology*, 61, 489-506 2015.

942 Malinverno, E., Maffioli, P., and Gariboldi, K.: Latitudinal distribution of extant fossilizable phytoplankton in the Southern
 943 Ocean: Planktonic provinces, hydrographic fronts and palaeoecological perspectives, *Marine Micropaleontology*, 123,
 944 41-58, doi: 10.1016/j.marmicro.2016.01.001, 2016.

945 Mitchell, C., Hu, C., Bowler, B., Drapeau, D., and Balch, W. M.: Estimating Particulate Inorganic Carbon Concentrations of
 946 the Global Ocean From Ocean Color Measurements Using a Reflectance Difference Approach, *Journal of Geophysical*
 947 *Research: Oceans*, 122, 8707-8720, doi: 10.1002/2017JC013146, 2017.

Formatted: Font: Italic

948 Mohan, R., Mergulhao, L. P., Guptha, M. V. S., Rajakumar, A., Thamban, M., AnilKumar, N., Sudhakar, M., and Ravindra,
 949 R.: Ecology of coccolithophores in the Indian sector of the Southern Ocean, *Marine Micropaleontology*, 67, 30-45, doi:
 950 10.1016/j.marmicro.2007.08.005, 2008.

951 Monteiro, F. M., Bach, L. T., Brownlee, C., Bown, P., Rickaby, R. E. M., Poulton, A. J., Tyrrell, T., Beaufort, L., Dutkiewicz,
 952 S., Gibbs, S., Gutowska, M. A., Lee, R., Riebesell, U., Young, J., and Ridgwell, A.: Why marine phytoplankton calcify,
 953 *Science Advances*, 2, e1501822, doi: doi:10.1126/sciadv.1501822, 2016.

954 [NASA Goddard Space Flight Center, Ocean Ecology Laboratory, Ocean Biology Processing Group. Moderate-resolution](#)
 955 [Imaging Spectroradiometer \(MODIS\) Aqua Level-2 Ocean Color, Version 2022 Data; NASA OB.DAAC, Greenbelt,](#)
 956 [MD, USA. doi: 10.5067/AQUA/MODIS/L2/OC/2022, 2022a \[Accessed on 10 July 2024\].](#)

957 NASA Goddard Space Flight Center, Ocean Ecology Laboratory, Ocean Biology Processing Group: Moderate-resolution
 958 Imaging Spectroradiometer (MODIS) Aqua Level-3 Mapped Particulate Inorganic Carbon, Version 2022 Data; NASA
 959 OB.DAAC, Greenbelt, MD, USA. doi: 10.5067/AQUA/MODIS/L3M/PIC/2022, 2022b [Access 01 June 2023].

960 NASA Ocean Biology Processing Group: Particulate Inorganic Carbon (PIC). Available from
 961 <https://oceancolor.gsfc.nasa.gov/resources/atbd/pic/>, 2023a [Access 14 June 2023].

962 Neukermans, G., Oziel, L., and Babin, M.: Increased intrusion of warming Atlantic water leads to rapid expansion of temperate
 963 phytoplankton in the Arctic, *Global Change Biology*, 24, 2545-2553, doi: 10.1111/gcb.14075, 2018.

964 Okada, H., and McIntyre, A.: Modern coccolithophores of the Pacific and North Atlantic oceans, *Micropaleontology*, 23, 1-
 965 54, doi: 10.2307/1485309 1977.

966 [Oliver, H., McGillicuddy, D. J., J., Krumhardt, K. M., Long, M. C., Bates, N. R., Bowler, B. C., Drapeau, D. T., and Balch,](#)
 967 [W. M.: Environmental drivers of coccolithophore growth in the Pacific sector of the Southern Ocean, *Global*](#)
 968 [Biogeochemical Cycles](#), 37(11), <https://doi.org/10.1029/2023GB007751>, 2023.

969 Orsi, A. H., and Harris, U.: Fronts of the Antarctic Circumpolar Current - GIS data, Ver. 1, Australian Antarctic Data Centre
 970 - https://data.aad.gov.au/metadata/records/antarctic_circumpolar_current_fronts, 2019 [Access 26 May 2023].

971 Orsi, A. H., Whitworth III, T., and Nowlin Jr, W. D.: On the meridional extent and fronts of the Antarctic Circumpolar Current,
 972 *Deep Sea Research Part I: Oceanographic Research Papers*, 42, 641-673, doi: 10.1016/0967-0637(95)00021-w, 1995.

973 Poulton, A. J., Young, J. R., Bates, N. R., and Balch, W. M.: Biometry of detached *Emiliana huxleyi* coccoliths along the
 974 Patagonian Shelf, *Marine Ecology Progress Series*, 443, 1-17, doi: 10.3354/meps09445, 2011.

975 Poulton, A. J., Painter, S. C., Young, J. R., Bates, N. R., Bowler, B., Drapeau, D., Lyczszkowski, E., and Balch, W. M.: The
 976 2008 *Emiliana huxleyi* bloom along the Patagonian Shelf: Ecology, biogeochemistry, and cellular calcification, *Global*
 977 *Biogeochemical Cycles*, 27, 1023-1033, doi: 10.1002/2013GB004641, 2013.

978 Reynolds, R. A., Stramski, D., and Mitchell, B. G.: A chlorophyll-dependent semianalytical reflectance model derived from
 979 field measurements of absorption and backscattering coefficients within the Southern Ocean, *Journal of Geophysical*
 980 *Research: Oceans*, 106, 7125-7138, doi: 10.1029/1999JC000311, 2001.

981 Rigual Hernández, A. S., Flores, J. A., Sierro, F. J., Fuertes, M. A., Cros, L., and Trull, T. W.: Coccolithophore populations
982 and their contribution to carbonate export during an annual cycle in the Australian sector of the Antarctic zone,
983 Biogeosciences, 15, 1843-1862, BG, 2018.

984 Rigual Hernández, A. S., Trull, T. W., Nodder, S. D., Flores, J. A., Bostock, H., Abrantes, F., Eriksen, R. S., Sierro, F. J.,
985 Davies, D. M., Ballegeer, A. M., Fuertes, M. A., and Northcote, L. C.: Coccolithophore biodiversity controls carbonate
986 export in the Southern Ocean, Biogeosciences, 17, 245-263, doi: 10.5194/bg-17-245-2020, 2020a.

987 Rigual-Hernández, A. S., Trull, T. W., Flores, J. A., Nodder, S. D., Eriksen, R., Davies, D. M., Hallegraeff, G. M., Sierro, F.
988 J., Patil, S. M., Cortina, A., Ballegeer, A. M., Northcote, L. C., Abrantes, F., and Rufino, M. M.: Full annual monitoring
989 of Subantarctic *Emiliania huxleyi* populations reveals highly calcified morphotypes in high-CO₂ winter conditions,
990 Scientific reports, 10, 2594, doi: 10.1038/s41598-020-59375-8, 2020b.

991 Rivero-Calle, S., Gnanadesikan, A., Del Castillo, C. E., Balch, W. M., and Guikema, S. D.: Multidecadal increase in North
992 Atlantic coccolithophores and the potential role of rising CO₂, Science, 350, 1533-1537, doi: 10.1126/science.aaa8026,
993 2015.

994 [Robertson, J. E., Robinson, C., Turner, D. R., Holligan, P., Watson, A. J., Boyd, P., Fernandez, E., & Finch, M. \(1994\), The](#)
995 [impact of a coccolithophore bloom on oceanic carbon uptake in the northeast Atlantic during summer 1991, Deep-Sea](#)
996 [Research Part I, 41\(2\), 297-314, doi:10.1016/0967-0637\(94\)90005-1.](#)

997 Rost, B., and Riebesell, U.: Coccolithophore calcification and the biological pump: response to environmental changes, in:
998 Coccolithophores: from molecular processes to global impact, edited by: Thierstein, H. R., and Young, J. R., Springer,
999 Berlin-Heidelberg, Germany, 99-125, 2004.

1000 Saavedra-Pellitero, M., Baumann, K.-H., Flores, J.-A., and Gersonde, R.: Biogeographic distribution of living
1001 coccolithophores in the Pacific sector of the Southern Ocean, Marine Micropaleontology, 109, 1-20, doi:
1002 10.1016/j.marmicro.2014.03.003, 2014.

1003 Saavedra-Pellitero, M., Baumann, K. H., Fuertes, M. Á., Schulz, H., Marcon, Y., Vollmar, N. M., Flores, J. A., and Lamy, F.:
1004 Calcification and latitudinal distribution of extant coccolithophores across the Drake Passage during late austral summer
1005 2016, Biogeosciences, 16, 3679-3702, doi: 10.5194/bg-16-3679-2019, 2019.

1006 Salter, I., Schiebel, R., Ziveri, P., Movellan, A., Lampitt, R., and Wolff, G. A.: Carbonate counter pump stimulated by natural
1007 iron fertilization in the Polar Frontal Zone, Nature Geoscience, 7, 885-889, doi: 10.1038/ngeo2285, 2014.

1008 Samtleben, C. and Schröder, A.: Living coccolithophore communities in the Norwegian-Greenland Sea and their record in
1009 sediments, Marine Micropaleontology, 19, 333-354, 1992.

1010 Schindelin, J., Arganda-Carreras, I., Frise, E., Kaynig, V., Longair, M., Pietzsch, T., Preibisch, S., Rueden, C., Saalfeld, S.,
1011 Schmid, B., Tinevez, J.-Y., White, D. J., Hartenstein, V., Eliceiri, K., Tomancak, P., and Cardona, A.: Fiji: an open-
1012 source platform for biological-image analysis, Nature Methods, 9, 676-682, doi: 10.1038/nmeth.2019, 2012.

1013 Schneider, C. A., Rasband, W. S., and Eliceiri, K. W.: NIH Image to ImageJ: 25 years of image analysis, Nature Methods, 9,
1014 671-675, doi: 10.1038/nmeth.2089, 2012.

Shutler, J. D., Land, P. E., Brown, C. W., Findlay, H. S., Donlon, C. J., Medland, M., Snooke, R., and Blackford, J. C.: Coccolithophore surface distributions in the North Atlantic and their modulation of the air-sea flux of CO₂ from 10 years of satellite Earth observation data, *Biogeosciences*, 10, 2699-2709, doi: 10.5194/bg-10-2699-2013, 2013.

Siegel, H., Ohde, T., Gerth, M., Lavik, G., and Leipe, T.: Identification of coccolithophore blooms in the SE Atlantic Ocean off Namibia by satellites and in-situ methods, *Continental Shelf Research*, 27, 258-274, doi: 10.1016/j.csr.2006.10.003, 2007.

Smyth, T. J., Moore, G. F., Groom, S. B., Land, P. E., and Tyrrell, T.: Optical modeling and measurements of a coccolithophore bloom, *Appl. Opt.*, 41, 7679-7688, doi: 10.1364/AO.41.007679, 2002.

Smyth, T. J., Tyrrell, T., and Tarrant, B.: Time series of coccolithophore activity in the Barents Sea, from twenty years of satellite imagery, *Geophysical Research Letters*, 31, doi: 10.1029/2004GL019735, 2004.

Suchéras-Marx, B., Viseur, S., Walker, C. E., Beaufort, L., Probert, I., and Bolton, C.: Coccolith size rules – What controls the size of coccoliths during coccolithogenesis?, *Marine Micropaleontology*, 170, 102080, doi: 10.1016/j.marmicro.2021.102080, 2022.

Trull, T. W., Passmore, A., Davies, D. M., Smit, T., Berry, K., and Tilbrook, B.: Distribution of planktonic biogenic carbonate organisms in the Southern Ocean south of Australia: a baseline for ocean acidification impact assessment, *Biogeosciences*, 15, 31-49, doi: 10.5194/bg-15-31-2018, 2018.

Tyrrell, T., and Taylor, A. H.: A modelling study of *Emiliania huxleyi* in the NE atlantic, *Journal of Marine Systems*, 9, 83-112, doi:10.1016/0924-7963(96)00019-X, 1996.

Vollmar, N. M., Baumann, K.-H., Saavedra-Pellitero, M., and Hernández-Almeida, I.: Distribution of coccoliths in surface sediments across the Drake Passage and calcification of *Emiliania huxleyi* morphotypes, *Biogeosciences*, 19, 585–612, <https://doi.org/10.5194/bg-19-585-2022>, 2022.

von Dassow, P., Díaz-Rosas, F., Bendif, E. M., Gaitán-Espitia, J. D., Mella-Flores, D., Rokitta, S., John, U., and Torres, R.: Over-calcified forms of the coccolithophore *Emiliania huxleyi* in high-CO₂ waters are not preadapted to ocean acidification, *Biogeosciences*, 15, 1515-1534, doi: 10.5194/bg-15-1515-2018, 2018.

Werdell, J., O'Reilly, J., Hu, C., Feng, L., Lee, Z., Franz, B., Bailey, S., Proctor, C., and Wang, G.: Chlorophyll a. NASA Algorithm Publication Tool, 2023-11-06, v1.1. Available from <https://www.earthdata.nasa.gov/documents/chlor-a/v1.1>, 2023, <https://doi.org/10.5067/JCQB8QALDOYD> [Access 20 July 2024]

Whitworth, T. I.: Zonation and geostrophic flow of the Antarctic circumpolar current at Drake Passage, *Deep Sea Research Part A. Oceanographic Research Papers*, 27, 497-507, doi: 10.1016/0198-0149(80)90036-9, 1980.

Winter, A., Elbrächter, M., and Krause, G.: Subtropical coccolithophores in the Weddell Sea, *Deep Sea Research Part I: Oceanographic Research Papers*, 46, 439-449, doi: 10.1016/S0967-0637(98)00076-4, 1999.

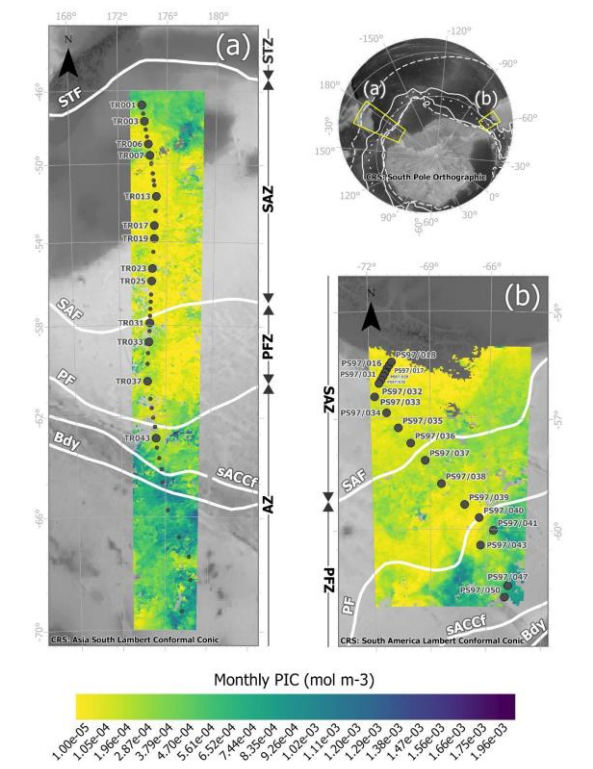
Winter, A., Henderiks, J., Beaufort, L., Rickaby, R. E. M., and Brown, C. W.: Poleward expansion of the coccolithophore *Emiliania huxleyi*, *Journal of Plankton Research*, 36, 316-325, 10.1093/plankt/fbt110, 2014.

1048 Yang, T. N., and Wei, K. Y.: How many coccoliths are there in a coccosphere of the extant coccolithophorids? A compilation,
1049 Journal of Nannoplankton Research, 25, 7-15, 2003.

1050 Young, J.: Coccobiom2 Macros, available from: <http://ina.tmsoc.org/nannos/coccobiom/Usernotes.html>, 2015 [Access 23
1051 August 2017]

1052 Young, J. R., and Ziveri, P.: Calculation of coccolith volume and it use in calibration of carbonate flux estimates, Deep Sea
1053 Research Part II: Topical Studies in Oceanography, 47, 1679-1700, doi: 10.1016/S0967-0645(00)00003-5, 2000.

1054 Young, J. R., Poulton, A. J., and Tyrrell, T.: Morphology of *Emiliania huxleyi* coccoliths on the northwestern European shelf
1055 – is there an influence of carbonate chemistry?, Biogeosciences, 11, 4771-4782, doi: 10.5194/bg-11-4771-2014, 2014.
1056



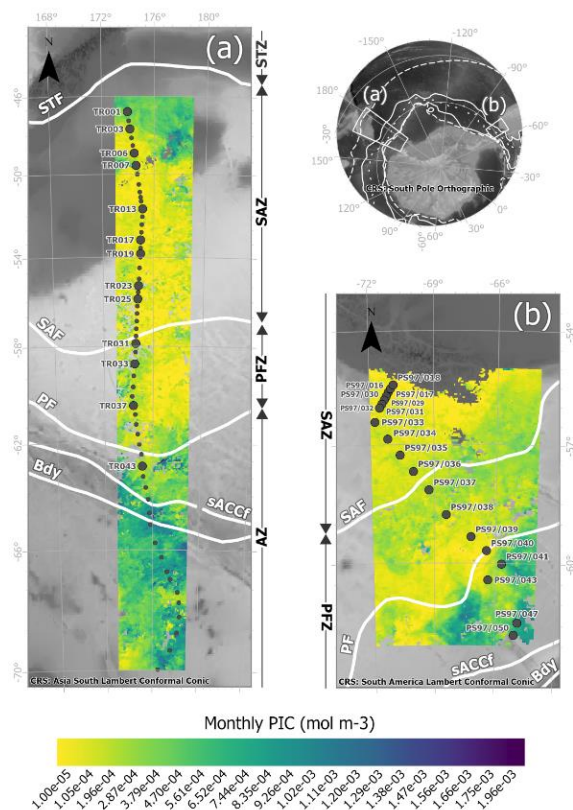


Figure 1: Study area showing the location of the water samples retrieved from (a) the New Zealand transect, collected during the XX Italian Expedition from New Zealand to Antarctica on board *R/V Italia* (December 2004-January 2005) and (b) the Drake Passage transect, collected during *Polarstern* Expedition PS97 across the Drake Passage (February-March 2016). **Large dots indicate samples in which biometries on *Emiliania huxleyi* were performed, and small dots where coccolithophore census were available.** The maps show **MODIS-Aqua L3 PIC concentrations in mol m⁻³ gsatellite-derived PIC-values (NASA Ocean Biology Processing Group 2022)** corresponding to (a) monthly mean over January 2005 and (b) monthly mean over February and March 2016, overlain on a bathymetry background (GEBCO Compilation Group, 2022). White lines indicate the **average position of the ACC fronts** (Orsi and Harris, 2019), from north to south these are: SAF (Subantarctic Front), PF (Polar Front), sACCF (Southern ACC Front) and Bdy (Southern Boundary). The Southern Ocean zones are labeled on the side of each map: STZ, Subtropical Zone; SAZ, Subantarctic Zone; PFZ, Polar Frontal Zone; AZ, Antarctic Zone.

Formatted: Font: Italic

Formatted: Font: Italic

Formatted: Font: Italic

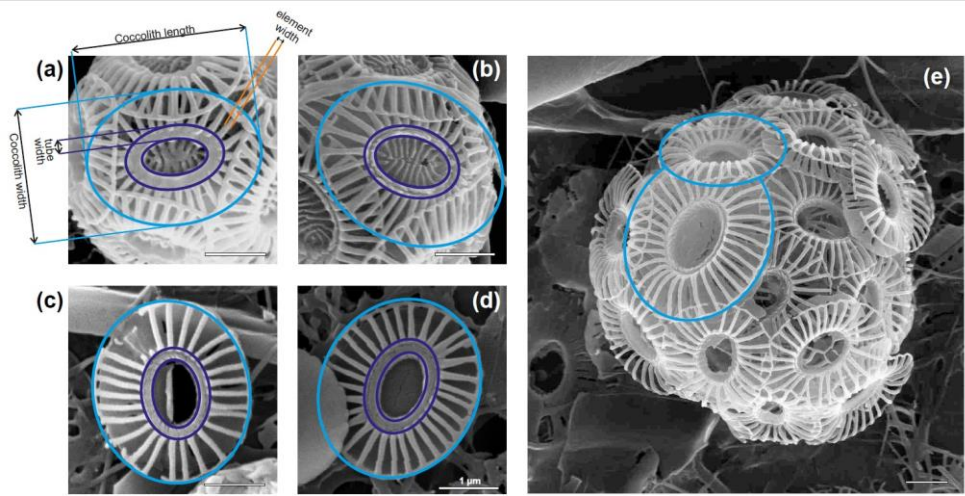


Figure 2: Parameters measured in *Emiliana huxleyi* coccoliths (a, b) type A and (c, d, e) type O in plankton samples from the New Zealand transect. Note the coccolith size variation in (e) within the same coccosphere.

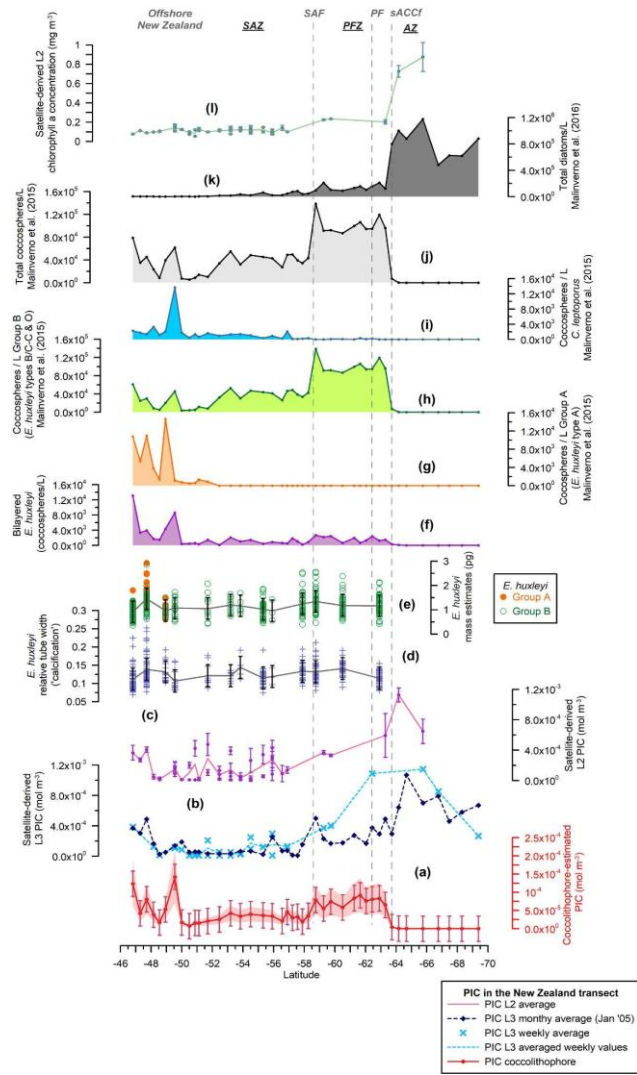


Figure 3: New Zealand transect showing (a) estimated total coccolithophore PIC (red line with dots) in mol m^{-3} , (b) MODIS-Aqua L3 PIC concentration values (mol m^{-3}), corresponding to a monthly average (January 2005, dark blue dashed line with diamonds),

1079 weekly average (~~electric-light~~ blue dashed line with ~~crossestriangles~~), (c) and ~~estimated total coccolithophore PIC (red line with~~
1080 ~~dots), all in mol m⁻³~~ MODIS-Aqua L2 PIC concentration values in mol m⁻³ (average in pink), (db) *Emiliana huxleyi* relative tube width² index (average in

1081 gray), (ee) *E. huxleyi* coccolith mass estimates (pg) for morphogroup A (dots) and B (circles) (average in gray), (fd) number of

1082 bilayered *E. huxleyi* (coccospheres/L), (ge) number of *E. huxleyi* morphogroup A (coccospheres/L), (hf) number of *E. huxleyi*

1083 morphogroup B (coccospheres/L), (ig) number of *Calcidiscus leptoporus* (coccospheres/L), (jh) Number of total coccolithophores

1084 (coccospheres/L) (~~Malinverno et al., 2015~~), (ki) Number of total diatoms (cells/L) (Malinverno et al., 2016), (l) (~~Malinverno et al.,~~

1085 ~~2015~~), MODIS-Aqua L2 chlorophyll a concentration in mg m⁻³ values (average in light green).

1086

1087 Note that the pPlankton samples were retrieved at ca. 3 m water depth. Vertical bars indicate one standard deviation on the entire

1088 population in (a), (d) and (e), and the standard deviation (considering a 5 x 5 window) in (c) and (l). The shaded area in (a) represents

1089 a 50% error.

1090 Vertical dashed lines indicate some of the ACC fronts (Orsi and Harris, 2019): SAF (Subantarctic Front), PF (Polar Front) and

1091 sACCf (Southern ACC Front). The Southern Ocean zones are labeled as SAZ (Subantarctic Zone), PFZ (Polar Frontal Zone) and

1092 AZ (Antarctic Zone).

1093

- Formatted: Font: Bold
- Formatted: Font: Bold
- Formatted: Font: Bold
- Formatted: Font: Bold
- Formatted: Font: Bold
- Formatted: Font: Bold
- Formatted: Font: Bold
- Formatted: Font: Bold
- Formatted: Font: Bold
- Formatted: Font: Bold
- Formatted: Font: Bold
- Formatted: Left

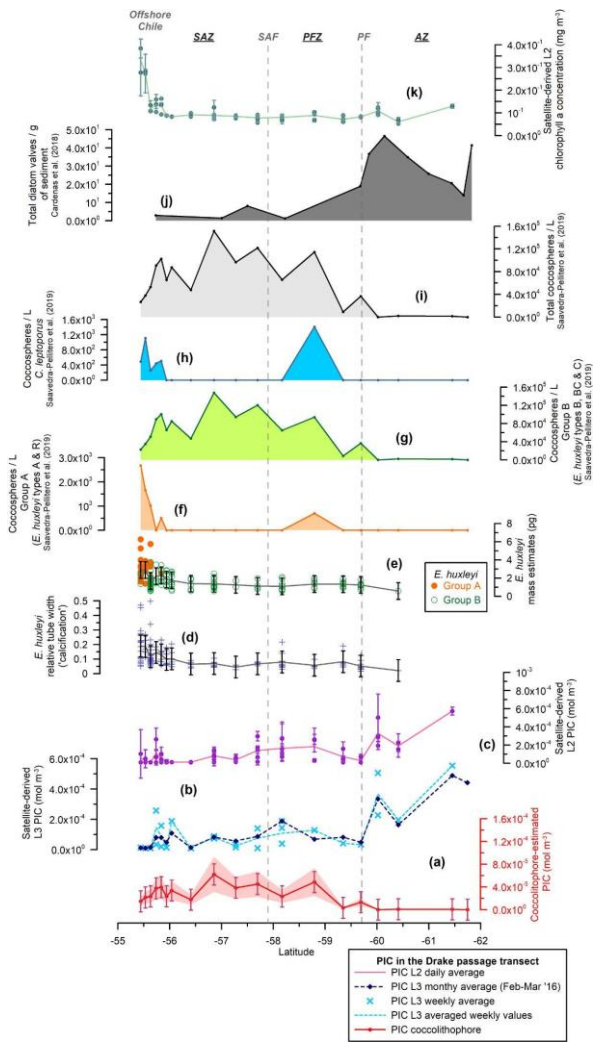


Figure 4: Drake Passage transect showing- (a) estimated total coccolithophore PIC (red line with dots) in mol m^{-3} , (b) MODIS-Aqua L3 PIC concentration (mol m^{-3}) corresponding to a monthly average (February and March 2016, dark blue dashed line with diamonds), weekly average (light blue dashed line with crosses), (c) MODIS-Aqua L2 PIC concentration in mol m^{-3} (average in pink), (d) satellite-derived

1099 PIC values (NASA Ocean Biology Processing Group, 2022) corresponding to a monthly average (February and March 2016, dark
1100 blue dashed line with diamonds), weekly average (electric light blue dashed line with triangles) and estimated total coccolithophore
1101 PIC (red line with dots), all in mol m^{-3} , (dh) *Emiliania huxleyi* relative tube width index² (average in gray), (ee) *E. huxleyi* coccolith
1102 mass estimates (pg) for morphogroup A (dots) and B (circles) in (pg) (average in gray), (fd) number of *E. huxleyi* morphogroup A
1103 (coccospheres/L), (ge) number of *E. huxleyi* morphogroup B (coccospheres/L), (hf) number of *Calcidiscus leptoporus*
1104 (coccospheres/L), (ig) Number of total coccolithophores (coccospheres/L) (Saavedra-Pellitero et al., 2019), (jh) Number of valves per
1105 gram of sediment from surface sediment samples across the Drake Passage and Scotia Sea (Cárdenas et al., 2018), (k) MODIS-Aqua
1106 L2 chlorophyll a concentration in mg m^{-3} (average in light green). Note that plankton samples were retrieved at 5, 10 and 20 m water
1107 depth. Note that plankton samples (a-g) were retrieved at 5, 10 and 20 m water depth. Vertical bars indicate one standard deviation on
1108 the entire population in (a), (d) and (e), and the standard deviation (considering a 5 x 5 window) in (c) and (k). The shaded area in (a)
1109 represents a 50% error. Vertical dashed lines indicate some of the ACC fronts (Orsi and Harris, 2019): SAF (Subantarctic Front) and
1110 PF (Polar Front). The Southern Ocean zones are labeled as SAZ (Subantarctic Zone), PFZ (Polar Frontal Zone) and AZ (Antarctic
1111 Zone).
1112

Formatted: Font: Not Bold

Formatted: Font: Not Bold

Formatted: Font: Not Bold

Formatted: Font: Not Bold

Formatted: Font: Not Bold

Formatted: Font: Not Bold

Formatted: Font: Not Bold

Formatted: Font: Not Bold

Formatted: Font: Not Bold

Formatted: Font: Not Bold

Formatted: Font: Not Bold

Formatted: Font: Not Bold

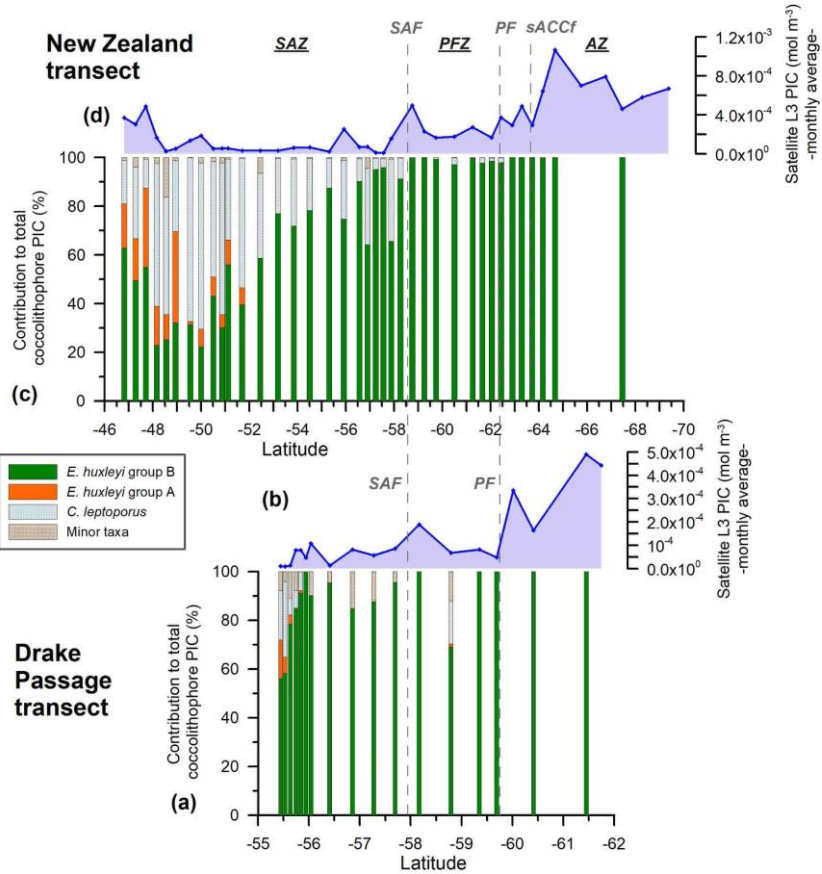
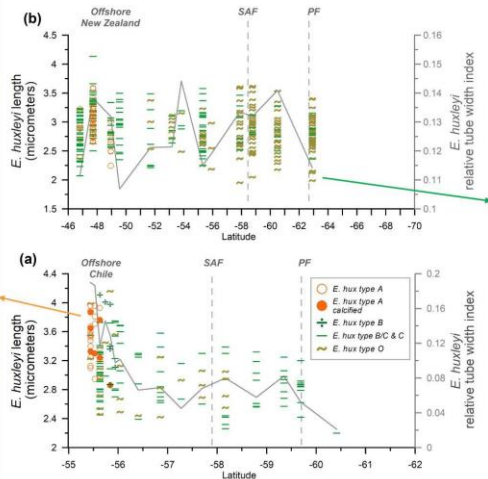
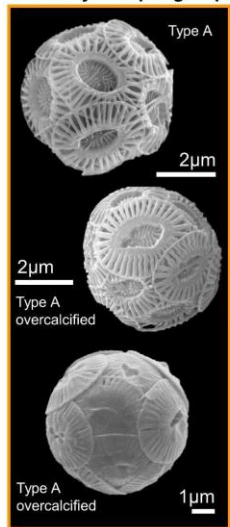


Figure 5: New Zealand (NZ) and Drake Passage (DP) transects showing (a, c) the relative PIC contribution of the different nanofloral taxa (*E. huxleyi* morphogroups A and B, *Calcidiscus leptoporus* and minor species) to the estimated coccolithophore PIC in 38 NZ and 17 DP samples bearing coccospheres; (b, d) MODIS-Aqua L3 monthly average satellite-derived PIC values (February and March 2016, dark blue line with diamonds) in mol m⁻³. Vertical dashed lines indicate some of the ACC fronts (Orsi and Harris, 2019): SAF (Subantarctic Front) and PF (Polar Front). The Southern Ocean zones are labeled as SAZ (Subantarctic Zone), PFZ (Polar Frontal Zone) and AZ (Antarctic Zone).

E. huxleyi morphogroup A



E. huxleyi morphogroup B

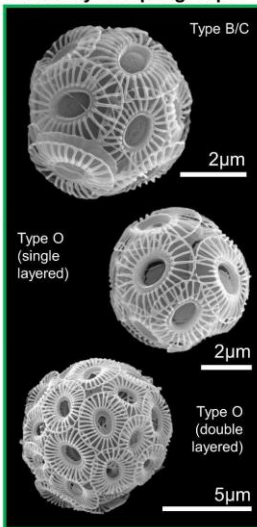
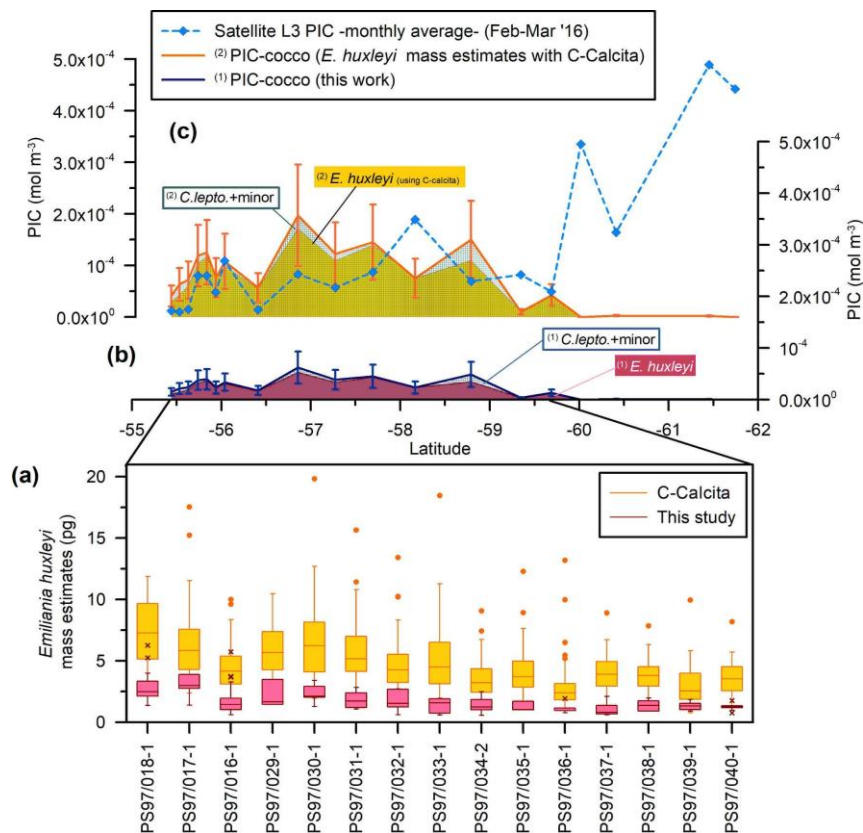


Figure 6: *Emiliania huxleyi* length (in μm) (indicated with different symbols depending on the type, and different colors depending on the morphogroup A or B) and averaged relative tube width² index (gray line) in (a) the Drake Passage and (b) New Zealand transects. On the left-hand side: pictures of coccospheres of *E. huxleyi* type A (within the morphogroup A) showing different degrees of calcification and on the right-hand side pictures of type B/C as well as type O belonging to the morphogroup B. All the [images of](#) coccospheres are from the New Zealand transect, except for the left bottom one, which was retrieved offshore of Chile.

1133
1134
1135
1136
1137
1138
1139
1140
1141
1142
1143

Figure 7: Principal component analysis (PCA) of the *E. huxleyi* morphometric dataset (including samples from both transects), log-transformed. This includes the coccolith length (major), the coccolith width (minor), the distal shield element width, the number of T-elements and the tube width measurements. Each coccolith measured has been labeled with its morphotype: A, A-overcalcified (both in orange), B, B/C-C (both in green) and O (in blue). All the SEM pictures of coecospheres are from samples retrieved in the Drake Passage transect except for (e), which is from the New Zealand transect.

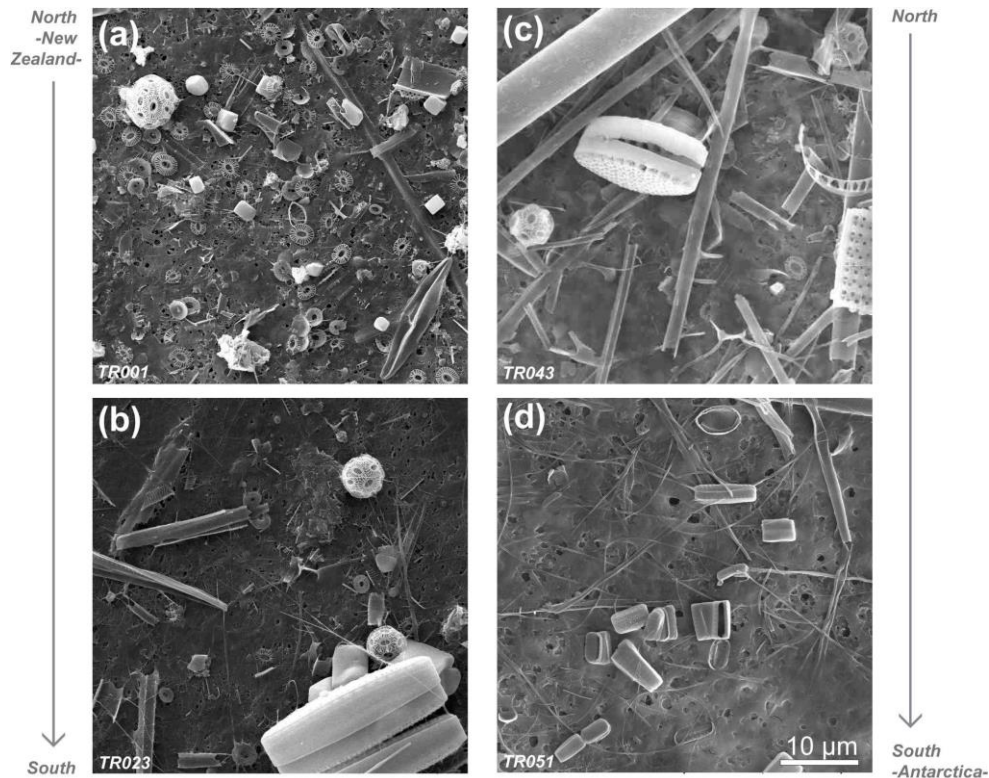
1144
1145



1146
1147
1148
1149
1150
1151
1152
1153
1154
1155
1156
1157
1158
1159

Figure 7: Drake Passage latitudinal transect showing (a) coccolith mass estimates box plots (in pg): in dark red plus pink for this study (outliers are indicated with “x”) and yellow plus orangeblue for Saavedra-Pellitero et al. (2019) (outliers are indicated with a dot); (b) MODIS L3 monthly average satellite-derived PIC values (dark blue dashed line with diamonds) and estimated coccolithophore PIC (PIC-cocco) (all in mol m⁻³) -this study (1)-; Contributions of different coccolith taxa or groups have been indicated (*C.lepto.* = *Calcidiscus leptoporus*); (c)- MODIS-Aqua L3 monthly average satellite-derived PIC values (blue dashed line with diamonds) and PIC-cocco calculated considering averaged *Emiliania huxleyi* mass estimates obtained with the software C-Calcita (2) (Saavedra-Pellitero et al., 2019). Note that the contributions of different coccolith taxa or groups have been indicated (*C.lepto.* = *Calcidiscus leptoporus*; minor = minor species) and that the data is stacked for each of the approaches. Vertical bars in (b) and (c) represent a 50% error. Note that the PIC-cocco has been calculated in two ways: (1) as indicated in this study and (2) considering averaged *Emiliania huxleyi* mass estimates obtained with the software C-Calcita (Saavedra-Pellitero et al., 2019). The data is only stacked for each of the approaches.

1160
1161



1162
1163
1164
1165
1166

Figure 89: SEM pictures of samples retrieved in the Subantartic Zone (a, b) and south of the Polar Front (c, d) in the New Zealand transect.

Table 1: Overview of the samples considered for this study, including the sampling area, number of plankton samples considered for this study, expedition, research vessel, water sampling dates, coordinates and data already available from previous publications.

Area	Number of samples considered for this work	Water depth (m)	Expedition	Research Vessel	Plankton sampling period	Coordinates	Previous publications
New Zealand	42	3	XX Italian Expedition	RV Italica	31.12.2004-06.01.2005	46.81°S to 69.98°S	Coccolithophore assemblages: Malinverno et al. (2015); Dinoflagellates, Coccolithophores, Silicoflagellates, Diatoms, Parmales, Archaeomonads and micro-zooplankton: Malinverno et al. (2016)
Drake Passage	19	5, 10 and 20	Expedition PS97	Polarstern	24.02.2016-05.03.2016	55.44°S to 61.75°S	Coccolithophore assemblages: Saavedra-Pellitero et al. (2019); <i>Emiliania huxleyi</i> mass estimantes: Saavedra-Pellitero et al. (2019)

1174
1175
1176
1177
1178
1179
1180
1181
1182

Table 24: Length, [shape factors](#) (Ks) and number of coccoliths per coccosphere used in this work for the New Zealand transect and the Drake Passage transect. (*) Indicates an average of the number of coccoliths per coccosphere. [Note that the different Ks used here were mostly based on Young and Ziveri \(2000\). The shape factor for morphotype O \(Ks = 0.015\) was introduced by Poulton et al. \(2011\) in a plankton study along the Patagonian Shelf for a morphotype with a central area described as an “open or thin plate” which the authors called type B/C but that we identified as morphotype O.](#)

Coccolithophore species	Average length ± standard deviation (µm) New Zealand	Average length ± standard deviation (µm) Drake Passage	Source	Ks	Source	Number of coccoliths per coccosphere N. Zealand	Number of coccoliths per coccosphere Drake P.	Source
<i>Calcidiscus leptoporus</i> spp. <i>leptoporus</i>	5.7±0.6	5.7±0.6	This work (biometries offshore N. Zealand)	0.08	Young and Ziveri (2000)	15	15	Kleijne (1993)
<i>Emiliana huxleyi</i> group A (average value)	2.95±0.28	3.49±0.33	This work	0.03	This work	15 single layered, 35 double layered	25 (*)	This work (own observations)
<i>Emiliana huxleyi</i> A overcalcified				0.04	Young and Ziveri (2000)			
<i>Emiliana huxleyi</i> A (normal)				0.02	Young and Ziveri (2000)			
<i>Emiliana huxleyi</i> group B (average value)	2.87±0.35	2.98±0.40	This work	0.02	Young and Ziveri (2000)			
<i>Emiliana huxleyi</i> B-B/C-C				0.02	Young and Ziveri (2000)			
<i>Emiliana huxleyi</i> O				0.015	Poulton et al. (2011)			
<i>Gephyrocapsa muelleriae</i>	3.9	3.9	Young and Ziveri (2000)	0.05	Young and Ziveri (2000)	15	15	Samtleben & Schroder (1992)
<i>Syracosphaera</i> spp.	2.2	5.5	Young and Ziveri (2000)	0.03	Young and Ziveri (2000)	25	25	Okada & McIntyre (1977)
Minor taxa			Young and Ziveri (2000)		Young and Ziveri (2000)			Yang & Wei (2003)

Coccolithophore species	Length (µm) New Zealand	Length (µm) Drake passage	Source	Ks	Source	Number of coccoliths per coccosphere N. Zealand	Number of coccoliths per coccosphere Drake P.	Source
<i>Calcidiscus leptoporus</i> spp. <i>leptoporus</i>	5	5	This work (biometries offshore N. Zealand)	0.08	Young and Ziveri (2000)	15	15	Kleijne (1993)
<i>Emiliana huxleyi</i> group A (average value)	2.95	3.49	This work	0.03	This work	15 single layered, 35 double layered	25 (*)	This work (own observations)
<i>Emiliana huxleyi</i> A overcalcified				0.04	Young and Ziveri (2000)			
<i>Emiliana huxleyi</i> A (normal)				0.02	Young and Ziveri (2000)			
<i>Emiliana huxleyi</i> group B (average value)	2.87	2.98	This work	0.02	Young and Ziveri (2000)			
<i>Emiliana huxleyi</i> B-B/C-C				0.02	Young and Ziveri (2000)			
<i>Emiliana huxleyi</i> O				0.015	This work			
<i>Gephyrocapsa muelleriae</i>	3.9	3.9	Young and Ziveri (2000)	0.05	Young and Ziveri (2000)	15	15	Samtleben & Schroder (1992)
<i>Syracosphaera</i> spp.	2.2	5.5	Young and Ziveri (2000)	0.03	Young and Ziveri (2000)	25	25	Okada & McIntyre (1977)
Minor taxa			Young and Ziveri (2000)		Young and Ziveri (2000)			Yang & Wei (2003)

Table 3. Summary of MODIS-Aqua products used in this study. ^(*)The first 8-day period of each year always begins with January 1, the second with January 9, the third with January 17, etc. The final "8-day" composite of each year comprises only five days in non-leap years (27 - 31 December) or six days in leap years (26 - 31 December) (NASA Ocean Biology Processing Group, 2018).

				Drake passage transect		New Zealand transect	
Satellite product	Biophysical variable	Extraction method	Time period	Time span	Num. of scenes	Time span	Num. of scenes
MODIS-A Level 2	■ PIC concentration (mol m ⁻³)	mean of 5x5 window centered on measurement location	Daily timestamp	17-02-2016 / 12-03-2016	50	24-12-2004 / 13-01-2005	34
	■ Chlorophyll a concentration (mg m ⁻³)						
MODIS-A Level 3	PIC concentration (mol m ⁻³)	value of pixel enclosing measurement location	8-daily ^(*) timestamp	10-02-2016 / 12-03-2016	4	26-12-2004 / 08/01/2005	2
MODIS-A Level 3	PIC concentration (mol m ⁻³)	value of pixel enclosing measurement location	Monthly timestamp	01-12-2004 / 31/01/2005	2	01-02-2016 / 31/03/2016	2

Supplementary material

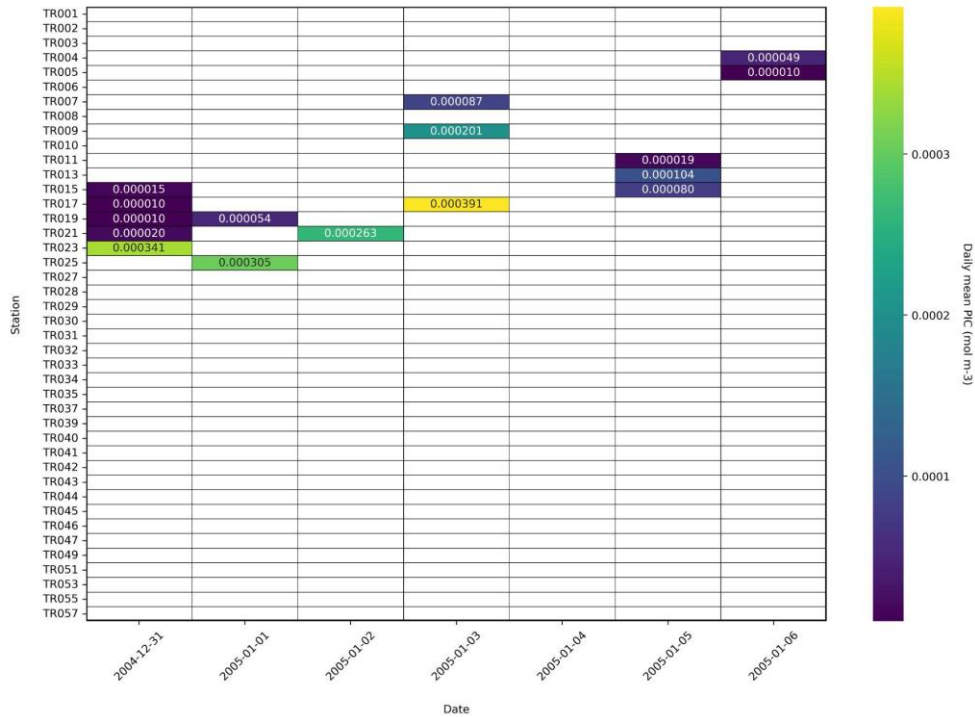
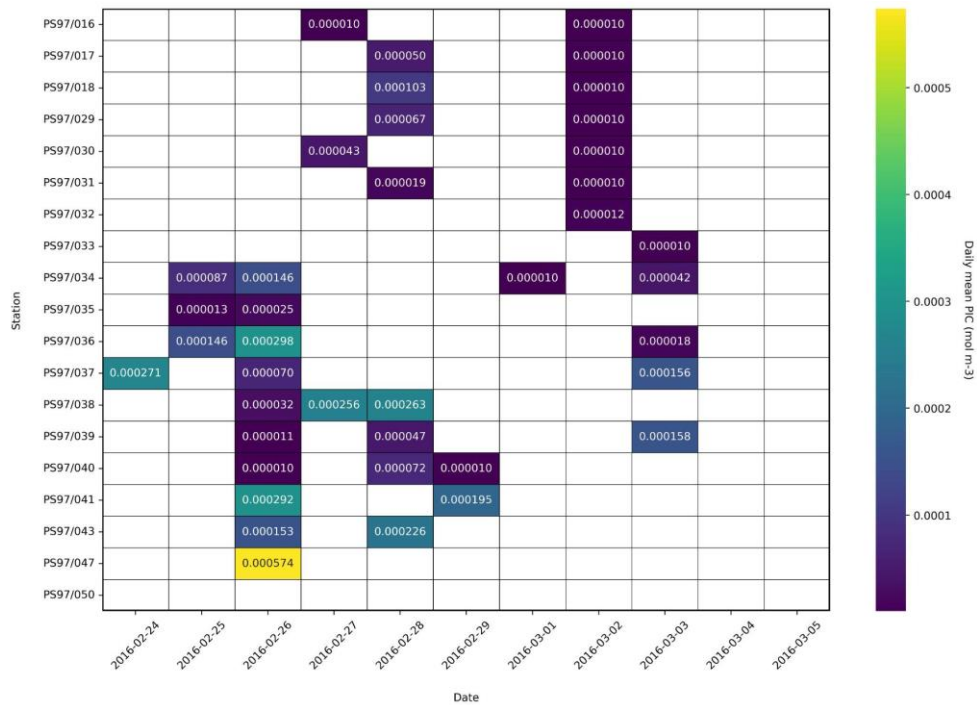


Figure 1S: Heatmap showing the MODIS-Aqua L2 PIC concentration values (mol m⁻³) for the New Zealand transect. Dates are shown in the X axis and stations (sorted by latitude, from North -up- to South -down-) in the Y axis. Note that the values on the labels are not logarithmic, but the colour scale is. The heatmap shows the availability and distribution of daily satellite-derived PIC concentrations.

1210



1211

1212

1213

1214

Figure 2S: Heatmap of MODIS-Aqua L2 PIC concentration values (mol m⁻³) for the Drake Passage transect. X axis shows Dates are shown in the X axis and stations (sorted by station name) in the Y axis. The heatmap shows the availability and distribution of daily satellite-derived PIC concentrations.

Formatted: Font: 17 pt

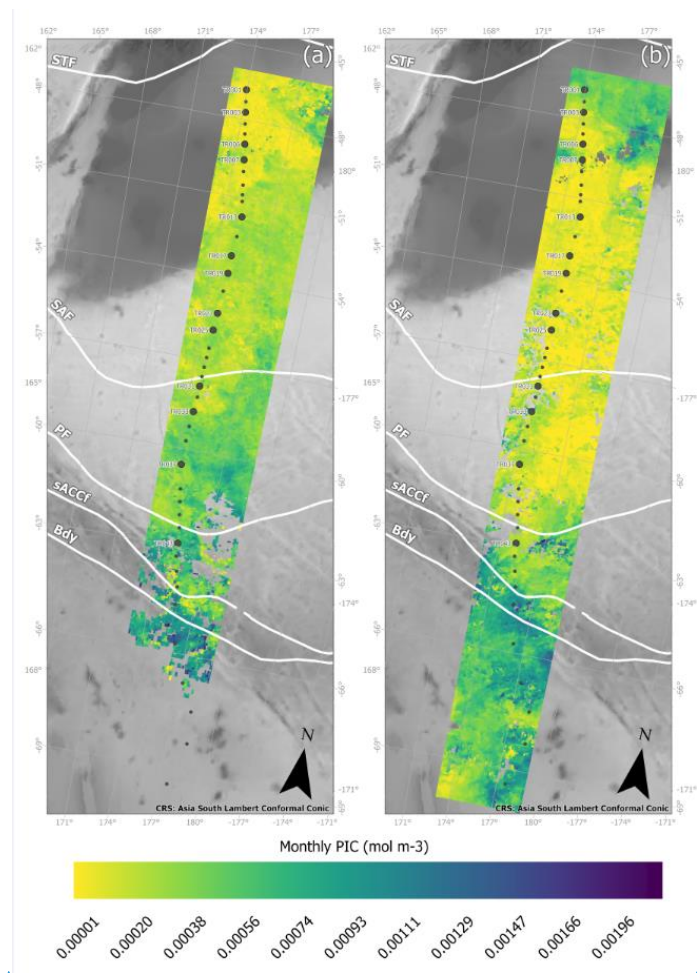


Figure 3S: Monthly MODIS-Aqua L3 PIC concentration values (mol m⁻³) in the New Zealand transect corresponding to (a) December 2004 and (b) January 2005, over a bathymetry background (GEBCO Compilation Group, 2022). White lines indicate the ACC fronts (Orsi and Harris (2019) from north to south: SAF (Subantarctic Front), PF (Polar Front), sACCF (Southern ACC Front) and Bdy (Southern Boundary). The Southern Ocean zones are labeled on the side of each map: STZ, Subtropical Zone; SAZ, Subantarctic Zone; PFZ, Polar Frontal Zone; AZ, Antarctic Zone.

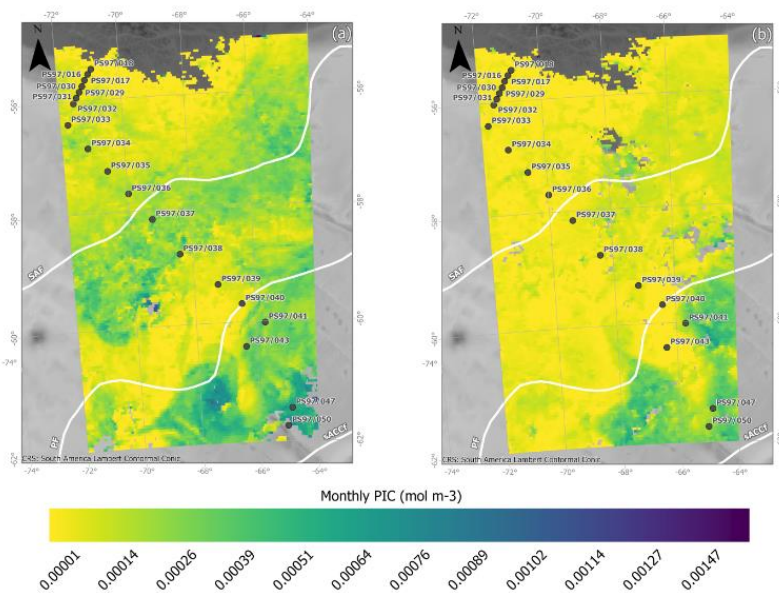


Figure 4S: Monthly MODIS-Aqua L3 PIC concentration values (mol m⁻³) in the Drake Passage corresponding to (a) February 2016 and (b) March 2016, over a bathymetry background (GEBCO Compilation Group, 2022). White lines indicate the ACC fronts (Orsi and Harris (2019) from north to south: SAF (Subantarctic Front), PF (Polar Front), sACCf (Southern ACC Front) and BdY (Southern Boundary). The Southern Ocean zones are labeled on the side of each map: STZ, Subtropical Zone; SAZ, Subantarctic Zone; PFZ, Polar Frontal Zone; AZ, Antarctic Zone.

Formatted: Font: 9 pt, Bold

Formatted: Font: 9 pt, Bold

Formatted: Font: 9 pt, Bold

Formatted: Font: 9 pt, Bold

Formatted: Font: 9 pt, Bold

Formatted: Font: 9 pt, Bold

Formatted: Font: 9 pt, Bold

Formatted: Font: 9 pt, Bold

Formatted: Font: 9 pt, Bold

Formatted: Font: 9 pt, Bold

Formatted: Font: 9 pt, Bold

Formatted: Font: 9 pt, Bold

Formatted: Font: 9 pt, Bold

Formatted: Font: 9 pt, Bold

Formatted: Font: 9 pt, Bold

Formatted: Font: 9 pt, Bold

Formatted: Font: 9 pt, Bold

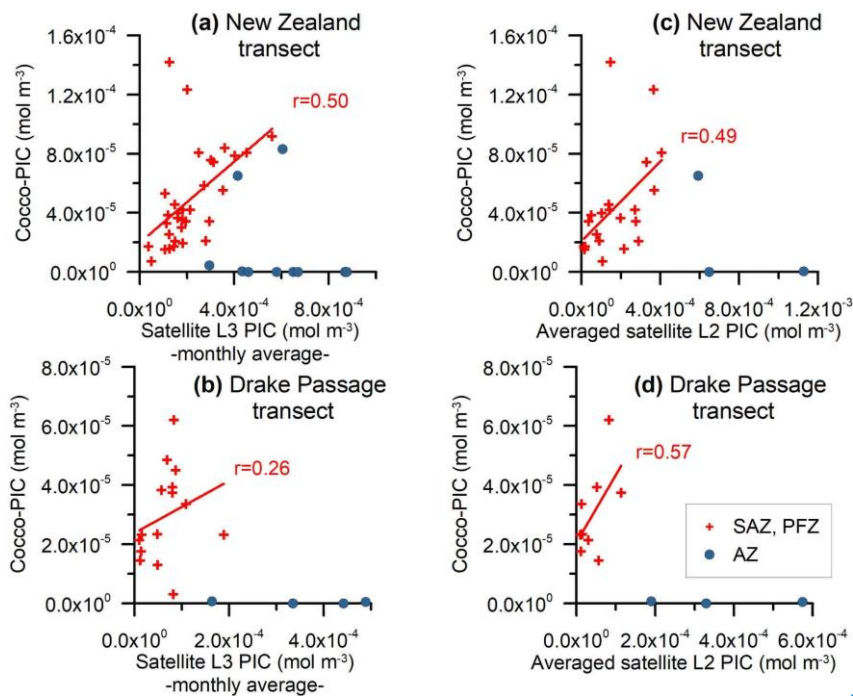
Formatted: Font: 9 pt, Bold

Formatted: Font: 9 pt, Bold

Formatted: Font: 9 pt, Bold

Formatted: Font: 9 pt, Bold

Formatted: Font: 9 pt, Bold



Formatted: Font: 9 pt, Bold

Formatted: Centered

Formatted: Font: 9 pt, Bold

Formatted: Font: 9 pt, Bold

Figure 5S: Monthly MODIS-Aqua L3 PIC values versus estimated total coccolithophore PIC for (a) the New Zealand and (b) Drake Passage transects (in mol m⁻³). Averaged MODIS-Aqua L2 PIC values versus estimated total coccolithophore PIC for the (c) the New Zealand and (d) Drake Passage transects (in mol m⁻³). The samples located in the Subantarctic Zone (SAZ) and Polar Frontal Zone (PFZ) have been indicated with crosses and those in the Antarctic Zone (AZ) with dots. A regression line and the Pearson correlation coefficient (r) has been indicated for those samples in the SAZ and PFZ.

Formatted: Left, Line spacing: single

Formatted: Font: 9 pt, Bold

Formatted: Font: 9 pt, Bold, Superscript

Formatted: Font: 9 pt, Bold

Formatted: Font: 9 pt, Bold

Formatted: Font: 9 pt, Bold

Formatted: Font: 9 pt, Bold, Superscript

Formatted: Font: 9 pt, Bold

Formatted: Font: 9 pt, Bold